LITHIUM COMPOUND CHARACTERIZATION VIA RAMAN SPECTROSCOPY AND LASER-INDUCED BREAKDOWN SPECTROSCOPY

THESIS

James T. Stofel, Captain, USAF

AFIT-ENP-MS-21-M-138

DEPARTMENT OF THE AIR FORCE
AIR UNIVERSITY

AIR FORCE INSTITUTE OF TECHNOLOGY

Wright-Patterson Air Force Base, Ohio

AFIT-ENP-MS-21-M-138

LITHIUM COMPOUND CHARACTERIZATION VIA RAMAN SPECTROSCOPY AND LASER-INDUCED BREAKDOWN SPECTROSCOPY

THESIS

Presented to the Faculty

Department of Engineering Physics

Graduate School of Engineering and Management

Air Force Institute of Technology

Air University

Air Education and Training Command

in Partial Fulfillment of the Requirements for the

Degree of Master of Science in Nuclear Engineering

James T. Stofel

Captain, USAF

March 2021

AFIT-ENP-MS-21-M-138

LITHIUM COMPOUND CHARACTERIZATION VIA RAMAN SPECTROSCOPY AND LASER-INDUCED BREAKDOWN SPECTROSCOPY

THESIS

James T. Stofel
Captain, USAF

Committee Membership:

Michael Shattan, LTC, Ph.D.
Chair

Anil Patnaik, Ph.D
Member

Andrew Giminaro, Ph.D
Member

AFIT-ENP-MS-21-M-138

Abstract

Industries such as lithium-ion battery producers and the nuclear industry community seek to produce and store lithium in pure chemical forms, such as lithium hydride (LiH) and anhydrous lithium hydroxide ($LiOH$) among others. However, these lithium compounds are reactive with the atmosphere and quickly degrade into less than desirable forms, including hydrogenous forms and lithium carbonate (Li_2CO_3). Therefore, industry desires a fast and effective quality control approach to quantify the ingrowth of these secondary lithium chemical forms. Additionally, in the field of forensics, there is a desire to determine storage/environmental conditions of lithium samples. This research seeks to compare the effectiveness of Raman spectroscopy and Laser-Induced Breakdown Spectroscopy (LIBS) in identifying lithium compounds in their pure form and in various mixtures. A pulsed laser and an echelle spectrograph are used in a novel single setup to conduct both measurements in tandem. The efficacy of these techniques for quantifying the relative ratios of the chemical forms in complex mixtures is then demonstrated and compared. Univariate and multivariate regression techniques including principal component regression and partial least squares regression were applied to both data sets to exploit the broad spectral nature of the echelle spectrograph. Analysis reveals the Raman data provides superior discrimination and regression fitting while the LIBS data provides only a moderate discrimination capability. However, Raman provides only surface analysis while LIBS provides an inherent depth profiling capability. Finally, this work proposed a novel Raman-LIBS configuration as a potential method to capitalize on the strengths of both techniques.

AFIT-ENP-MS-21-M-138

To my incredible wife, thank you for your undying love and support. Without you, my greatest successes in this life are meaningless to me.

To our daughter, our little bundle of joy, my experience at AFIT would not have been the same without you.

Acknowledgements

I would like to acknowledge the patient guidance of my committee as well as the lab supervisor and technicians I worked with closely.

James T. Stofel

Table of Contents

Page

Abstract iv

Dedication v

Acknowledgements vi

List of Figures ix

List of Tables xii

I. Introduction 1

1.1 Motivation 1
1.2 Background 2
1.2.1 Lithium Compounds of Interest 2
1.2.2 Raman 3
1.2.3 LIBS 4
1.2.4 Chemometrics 4
1.3 Problem 5
1.4 Hypothesis 5
1.5 Approach 6
1.6 Assumptions and Limitations 7

II. Theory and Literature Review 8

2.1 Other Techniques Used to Study Lithium Compounds 8
2.1.1 X-Ray Diffraction (XRD) 8
2.1.2 X-Ray Photoelectron Spectroscopy (XPS) 9
2.1.3 Fourier Transform Infrared (FTIR) and Diffuse Reflectance Infrared Fourier Transform (DRIFT) 9
2.2 Raman Spectroscopy 9
2.3 LIBS 12
2.3.1 Laser Ablation 14
2.3.2 Depth Profiling 16
2.3.3 Potential Challenges 16
2.4 Lithium Spectra 18
2.4.1 Raman Spectra of Lithium Compounds 18
2.4.2 LIBS Spectra of Lithium Compounds 21
2.5 Data Fusion 23
2.6 Univariate Regressions 24
2.7 Chemometrics 24
2.7.1 Principal Components Regression (PCR) 25
2.7.2 Partial Least Squares Regression (PLSR) 26

Page

III. Methodology 28

3.1 Sample Selection and Preparation 28
3.1.1 Pellet Pressing Procedure 29
3.2 Dual Setup 33
3.2.1 Echelle Spectrograph for Raman and LIBS 34
3.3 Raman 36
3.4 LIBS 39
3.4.1 Depth Profiling 40
3.5 Data Processing 41
3.5.1 Raman-LIBS Data Fusion 41
3.5.2 Univariate and Multivariate Analysis 42

IV. Results and Analysis 44

4.1 Raman 44
4.1.1 Univariate Regression 45
4.1.2 Pure Lithium Compounds 46
4.1.3 PCR/PLSR 46
4.2 LIBS 49
4.2.1 Univariate Regression 49
4.2.2 PCA on Pure Lithium Compounds 51
4.2.3 PCR/PLSR 51
4.2.4 Depth Profiling 54
4.3 Data Fusion: A Pseudo-Spectra 57
4.3.1 PCR/PLSR 57
4.4 Trends 59
4.5 A Concerning Observation 60

V. Conclusions 62

5.1 Recommendations for Future Work 63

Appendix A. Study on Pellet Pressing Parameters for analysis of $LiOH(H_2O)$ via LIBS 65

Bibliography 72

List of Figures

Figure		Page
1	A schematic of a typical Raman spectroscopy setup.	11
2	Rayleigh, Stokes Raman and anti-Stokes Raman frequency changes.	12
3	An example of a standard LIBS setup.	13
4	The energy level diagram for lithium.	14
5	The ablation process broken into three major steps.	15
6	Diagram illustrating the origin of self-absorption.	17
7	Raman spectra of LiH as obtained by Maupoix et al. in a study on the grain-size dependence of the hydrolysis of LiH.	19
8	Raman spectra of $LiOH$ as obtained by Gorelik et al.	20
9	Raman spectra of Li_2CO_3 as obtained by Brooker and Wang.	20
10	Simulated LIBS spectra approximating a 50/25/25 mixture of $LiH, LiOH, \& Li_2CO_3$ in a nitrogen atmosphere.	23
11	Scree plot of variance explained per principal component (bar chart) and total variance explained by sum of principal components (line plot). To be used in deciding how many principal components to use in analysis (theoretical data for conceptual purposes).	26
12	The glove box and equipment for creating samples prior to pressing a batch of pellets containing LiH and $LiOH$.	31
13	The pure Li_2CO_3 pellet which broke upon removal from the pellet press die on which it is sitting in this figure.	32
14	Conflat flange sample cell with UV fused silica viewport. The spacer is used to extend the distance between the focal point of the laser and the glass to avoid damage to the viewport.	33

Figure Page

15 The dual purpose setup used for both LIBS and Raman spectroscopy. . . . 35

16 Image of a deuterium/tungsten and halogen lamp taken with the echelle spectrograph. . . . 36

17 Sample and position numbering as used in Raman measurements. . . . 37

18 A single Raman spectra from each of three pure samples shows good distinction between the lithium compounds, though LiH is faintly visible on this scale. . . . 38

19 This zoomed-in Raman spectra allows for qualitative confirmation of the LiH Raman signal. . . . 38

20 This is a single-shot spectra of pure LiH over the bandwidth captured for LIBS measurements. . . . 40

21 Univariate regression for $LiOH$ in LiH using ratio of respective molecular Raman lines. . . . 45

22 Univariate regression for Li_2CO_3 in $LiOH$ using ratio of respective molecular Raman lines. . . . 46

23 Demonstrating separation between Raman spectra of pure lithium compounds in principal components space. . . . 47

24 Comparison of Raman data using PCR and PLSR for predicting percent concentration of $LiOH$ in LiH. . . . 48

25 Comparison of Raman data using PCR and PLSR for predicting percent concentration of Li_2CO_3 in $LiOH$. . . . 48

26 Univariate regression for $LiOH$ in LiH as a function of oxygen (777 nm) and hydrogen (656 nm). . . . 49

27 Univariate regression for Li_2CO_3 in $LiOH$ using ratio of oxygen (777 nm) and hydrogen (656 nm). . . . 50

28 The relative standard deviation of the integrated line intensity for oxygen is the primary contributor to the variance in the R1 univariate regression values. . . . 51

Figure Page

29 Demonstrating separation between LIBS spectra of pure lithium compounds in principal components space. 52

30 Comparison of LIBS data using PCR and PLSR for predicting percent concentration of $LiOH$ in LiH. 53

31 Comparison of LIBS data using PCR and PLSR for predicting percent concentration of Li_2CO_3 in $LiOH$. 53

32 A comparison of two LIBS spectra from the same sample just a few shots apart shows dramatic changes attributable to matrix effects in the sample. 55

33 Comparison of fusion data using PCR and PLSR for predicting percent concentration of $LiOH$ in LiH. 58

34 Comparison of fusion data using PCR and PLSR for predicting percent concentration of Li_2CO_3 in $LiOH$. 58

35 Dark charring marks on pure LiH samples indicative of thermal reactions, photochromism or both. 61

List of Tables

Table		Page
1	A list of the Raman lines of interest for lithium compounds in this study.	19
2	List of elements and their primary atomic lines of interest.	22
3	Concentration of Lithium Compounds in Samples of this Study	29
4	Equipment parameters for Raman measurements.	37
5	Equipment parameters for LIBS measurements.	39
6	Results of depth measurements from 10 ablation craters after 20 ablations in each crater.	54
7	Performance metrics across all measurement and analysis combinations.	59

LITHIUM COMPOUND CHARACTERIZATION VIA RAMAN SPECTROSCOPY AND LASER-INDUCED BREAKDOWN SPECTROSCOPY

I. Introduction

Lithium compounds are used in a variety of industries ranging from batteries, to pharmaceuticals, to nuclear weapons and everything in between [1–4]. Of particular interest are LiH, $LiOH$, and Li_2CO_3. The latter two are formed when the first reacts with air in various reaction pathways. These reactions lead to degradation in the material composition which further leads to decrease in performance in their intended uses. A fast and non-destructive method is desired by industries and other stakeholders for quantifying the extent of the degradation present in lithium compounds. In this work, two spectroscopic measurement techniques and several analytical approaches are explored for use in the above-mentioned application. The two measurement techniques are Laser-Induced Breakdown Spectroscopy (LIBS) and Raman spectroscopy. The analytical approaches include univariate analysis as well as multivariate analysis such as Principal Components Regression (PCR) and Partial Least Squares Regression (PLSR). While hydrolysis of lithium hydride to form lithium hydroxide has been studied to a great extent, there are far fewer studies of lithium carbonate as it relates to lithium hydride and hydroxide [5–16]. The inclusion of lithium carbonate in this study is of particular interest to some stakeholders.

1.1 Motivation

Lithium hydride is used in a variety of applications from hydrogen storage to nuclear weapons [5, 9]. LiH has been studied for use in life preserving buoyancy

devices due to its ability to rapidly provide gaseous hydrogen upon contact with water [2]. It has also shown great promise as a coolant for hypersonic flight [17]. In conjunction with depleted uranium, it has also been used as a moderator in nuclear reactors [1]. However, using LiH does not come without difficulty. The primary challenge with LiH is that it reacts with constituents of the air, namely H_2O and CO_2, to form $LiOH$, Li_2O and Li_2CO_3 [18]. The formations of Li_2O and $LiOH$ have been studied extensively since the 1950s, but much less is known about the formation of Li_2CO_3 [5, 9, 12, 19–22]. A greater understanding of the formation of lithium carbonate from lithium hydride, lithium hydroxide, and lithium oxide would allow for enhanced optimization of storage conditions. In the case of forensics analysis, this understanding could improve the capability to determine the storage conditions at a sample's origin. The first step in studying the relationship between lithium carbonate, lithium hydroxide, lithium oxide, and lithium hydride is determining which analysis technique is best suited for distinguishing the compounds from one another in a sample containing one or all of them. This work seeks to compare the effectiveness of LIBS and Raman in completing this task.

1.2 Background

1.2.1 Lithium Compounds of Interest

As stated above, the formation of lithium hydroxide and lithium oxide from lithium hydride has been studied heavily since the 1950s. LiH is the lightest solid hydrogen storage material known to man, which makes it a prime candidate for many applications of hydrogen storage where weight is of concern (e.g. space exploration). However, its usefulness is limited by its strong tendency to react with moisture in the environment. For this reason, the reactions between LiH and moisture have been studied heavily. While the formation of Li_2CO_3 has been noted in multiple studies,

in the context of surface barriers [22] and as a natural contaminant [21], its formation has not been well characterized.

The reaction known to produce lithium hydroxide is described by the following equation:

$$LiH + H_2O \longrightarrow LiOH + H_2 \tag{1}$$

It has been observed at the boundary layer between the $LiOH$ and LiH the following reaction occurs:

$$LiOH + LiH \longrightarrow Li_2O + H_2 \tag{2}$$

The formation of lithium carbonate follows the reactions in Eqn 3 and 4.

$$Li_2O + CO_2 \longrightarrow Li_2CO_3 \tag{3}$$

$$2LiOH + CO_2 \longrightarrow Li_2CO_3 + H_2O \tag{4}$$

Thus, one can see the in-growth of lithium carbonate in a lithium hydride sample is dependent on the sample first being exposed to moisture [22]. There is a critical need to measure the concentrations of different compounds both at the surface and at various layers of the sample. This can be accomplished by performing depth profiling on pressed pellets of the lithium compounds of interest.

1.2.2 Raman

The Raman technique relies on off-resonant, nonlinear scattering to determine molecular composition of a sample. Raman scattering is much less intense than the dominant scattering mechanism known as Rayleigh scattering. Because of this, Raman spectroscopy requires long integration times and special light rejection techniques to view the Raman spectral lines without other light saturating the camera.

No special treatment of the spectra is needed to determine the molecular composition of the sample. However, Raman spectroscopy does not lend itself to depth profiling like LIBS does.

1.2.3 LIBS

Laser-induced breakdown spectroscopy is a technique which uses a pulsed laser focused on a sample of interest. The high irradiance generates a laser induced plasma (LIP). The light which emits from the plasma is characteristic of the elements present in the plasma. This light is directed, using optical mirrors, lenses, and fibers, into a spectrometer which separates the spectral lines by wavelength in physical space. The intensity of each wavelength is measured by a camera and thus a spectra is recorded. The ratios of these lines to one another can be used to determine relative concentrations of each element present in the sample. Many factors impact the atomic spectral lines' relative intensities; these factors must be carefully controlled in order for this method to be successful. LIBS can also be used for depth profiling: a layer-by-layer analysis of the sample.

1.2.4 Chemometrics

Chemometrics, as used in this study, is "the chemical discipline that uses mathematical and statistical methods to provide maximum chemical information by analyzing chemical data" [23]. The statistical methods employed in extracting information from the LIBS and Raman spectra in this study are PCR, PLSR, and Principal Components Analysis (PCA). The information being sought is a model for predicting how much of each lithium compound is present in the sample being analyzed. The results of these chemometric techniques will be used to determine whether LIBS, Raman spectroscopy, or a data fusion of the two is best suited for creating this model.

Chemometrics has been used with LIBS extensively and has proven as a viable method for extracting information from a sample in question [24, 25]. Predictive models for molecular information have been created as well, provided the sample under analysis is known to only contain molecules which have been accounted for in the model [24–28]. This is possible because various combinations of molecular composition will have corresponding spectra with ratios of atomic emission peaks indicative of that mixture.

1.3 Problem

This research addresses the issue of whether Raman spectroscopy, LIBS or a data fusion of the two is best suited for quantifying the presence of the specific lithium compounds mentioned above. Special interest is placed on the quantification of lithium carbonate, however some samples were produced and analyzed which did not contain any of this compound. Including these non-carbon containing compounds provides verification that the method is capable of distinguishing between those samples with and without carbonate. The results of this work will be critical to the research focusing on quantifying these compounds following exposure to various environmental and storage conditions.

1.4 Hypothesis

It is hypothesized that both LIBS and Raman will effectively characterize lithium compounds in pressed pellets in this study. This hypothesis is based on the aforementioned success of others that have demonstrated that LIBS can be used for molecular composition analysis, particularly when the spectra are analyzed using chemometrics, though chemometrics may not be necessary [24, 28]. Raman spectroscopy, by its very nature provides a spectra that is molecule specific [29]. Regression models can be

built from data collected using both methods on samples of known lithium compound concentrations. Once a model has been developed using these known concentrations, a sample with unknown concentrations can be analyzed using that model to estimate the molecular makeup/concentration.

All else equal, Raman spectroscopy will likely provide a much better model (higher confidence, lower uncertainty) than LIBS for lithium compounds characterization. But LIBS provides the ability to perform depth profiling where Raman is a surface only technique. The use of both methods in tandem could prove to be better than either on their own.

1.5 Approach

The lithium compounds of interest are LiH, $LiOH$, and Li_2CO_3. The parent lithium compound is LiH and the others are products of LiH reacting with H_2O and CO_2 in the environment. Various mixtures of these compounds were created and then pressed into pellets for analysis.

Second, Raman spectroscopy was employed on the pellets. Raman spectroscopy was performed before LIBS because it is imperative the spectra be taken from a pristine sample. While LIBS is mostly nondestructive, the ablation process does perturb the surface of the samples which would then influence further measurements. Since Raman spectroscopy relies purely on scattering light, the samples are unaltered by performing this technique.

Third, LIBS was performed on the samples. Special care was taken to ensure each position under analysis was unperturbed by any other ablation site.

Finally, the LIBS and Raman data were analyzed using univariate techniques, PCR, PLSR, and PCA.

1.6 Assumptions and Limitations

This study makes some underlying assumptions about the sample composition and quality/accuracy of laboratory equipment used. While the purity of the samples is stated by the manufacturer, the impurities are not tabulated and are not quantified. Therefore, this study assumes the presence of impurities has a negligible effect on the analytical utility of the collected spectra. However, the presence of some impurities was evident. They are present in every spectra but do not interfere with any of the lines of interest and are therefore ignored. Additionally, the lamps used for calibrating the spectrometer are assumed to be accurate both in wavelength and temperature.

The limitations in this study, like the assumptions, are tied to the laboratory equipment. The light throughput for the atomic emission line of carbon at 833 nm is limited by the efficiency of the optical fiber and spectrometer at this wavelength. The stronger emission lines of carbon (247 nm and 909 nm) are outside the working range of both the optical fiber and spectrometer available for this study. The carbon line at 833 nm is significantly weaker (factor of $\sim$34) than the emission line at 247 nm and significantly lower than the emission intensities of any other lines of interest. Consequently, atomic carbon emission lines are rarely observed in the LIBS spectra obtained from samples containing Li_2CO_3.

II. Theory and Literature Review

When lithium hydride is exposed to moisture it reacts violently and releases gaseous hydrogen. This reaction is defined in Eqn 1 and is the reason why LiH must be handled in a controlled environment. The release of gaseous hydrogen creates a hazard for spontaneous combustion [18, 30]. Once lithium hydroxide has been produced by this reaction, the following reaction in Eqn 4 follows. It has been shown that Li_2O forms at the boundary layer between LiH and $LiOH$ [6]. This reaction is described in Eqn 2. It has also been shown that LiH samples pre-treated with exposure to H_2O, followed by exposure to CO_2 have a 50% reduction in subsequent reaction rate between LiH and H_2O [22]. A reduction in the rate of occurrence of the reaction in Eqn 2 has also been demonstrated in LiH samples pre-treated with exposure to CO_2 [6].

2.1 Other Techniques Used to Study Lithium Compounds

Lithium hydride and its hydrolysis products have been studied using several other analytical techniques other than LIBS and Raman spectroscopy, a few of which are described below.

2.1.1 X-Ray Diffraction (XRD)

XRD is an analytical technique that uses the principle of diffraction and applies it to crystalline samples. X-rays are imparted on a sample and the crystalline structures act as a 3-D diffraction grating. Through constructive and destructive interference, the observed pattern is indicative of particular structures which can then be identified [31, 32]. This technique is primarily used for identifying crystalline structures but can be used indirectly to provide elemental information [33]. Shuai used XRD

to observe the hydrolysis products of LiH when exposed to low relative humidity in argon atmosphere [5]. The results showed products resulting from the reactions represented in Eqn (1 - 2).

2.1.2 X-Ray Photoelectron Spectroscopy (XPS)

XPS is similar to XRD. It uses the same geometry except instead of measuring the x-rays being diffracted by the crystalline structure, it measures the photoelectrons emitted by the sample. X-ray are imparted on the sample. Those x-rays excite the electrons in the sample to the point where a fraction are emitted. The energy of the electron is a function of the incident x-ray energy and the binding energy of the electron to the atom where it originated [34]. Because these binding energies are discrete, elemental analysis can be conducted. This method of analysis was used by Chu et al. for quantification of LiH, $LiOH$, Li_2O, and Li_2CO_3 [6].

2.1.3 Fourier Transform Infrared (FTIR) and Diffuse Reflectance Infrared Fourier Transform (DRIFT)

FTIR and DRIFT (a subset of FTIR) illuminate the sample with a broadband infrared light source and measure the reflected light. The wavelengths of interest are in the infrared range (approximately 2500 nm) and thus special optics and detection equipment are required for this analysis technique [35]. FTIR and DRIFT have been used by Guichard et al., Matt et al. and others for the study of lithium hydride and its hydrolysis products [7, 8].

2.2 Raman Spectroscopy

Raman spectroscopy is a method for identifying the molecules present in a sample. This is accomplished by observing the scattered light from molecular vibrations

and rotations which follow excitation from a monochromatic light source. Unlike LIBS, Raman does not require breakdown of the material. In fact, breakdown of the material must be avoided in order for this method to be performed successfully. Raman scattering is named after the man who discovered the phenomena, Sir Chandrasekhara Venkata Raman. C. V. Raman discovered that when light is incident on a material a small portion of that light interacts through inelastic scattering. That is, there is light that is scattered which does not return with the same wavelength or intensity as the incident light [29, 36].

Inelastic scattering is a nonlinear optical process which occurs when the incident light interacts with a molecular state and transitions it to a new molecular state via a virtual state – involving absorption of the incident light and emission of light of different colors. The process is nearly instantaneous and occurs on the same timescale as the dominant Rayleigh scatter. Rayleigh scattering is when the scattered light is of the same wavelength and energy as the incident light. Typically, Raman scattering only occurs approximately on in ten million scatters [29]. This poses a challenge with respect to detection. With inelastic scattering rates this low, any device attempting to observe and measure these Raman emissions would be saturated by the Rayleigh scatter long before the Raman lines come into limits of detection [29]. With special notch filters that reject light of select wavelengths, it has become possible to view Raman lines with common detection cameras such as an Intensified Charge-Coupled Device (ICCD). A schematic of a typical Raman spectroscopy setup is shown in Figure 1.

Here, the Raman scattering process is described in further detail. When the rotational-vibrational (ro-vibronic) state of the molecule is excited with a transition to a virtual energy state, which is followed by a transition to another molecular energy state emitting a blue-shifted or red-shifted light; these transitions are called anti-

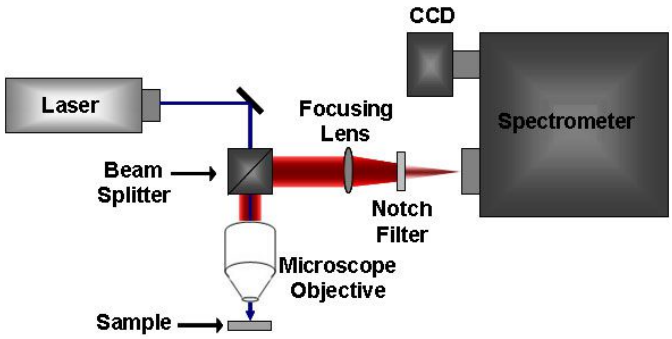

Figure 1. A schematic of a typical Raman spectroscopy setup [37].

Stokes and Stokes Raman scattering. Anti-Stokes emission lines will have a higher energy than the incident light and thus a shorter wavelength. The opposite will be true for Stokes lines [38]. Figure 2 provides a visual for Rayleigh, Stokes Raman, and anti-Stokes Raman scattering.

There are many categories for the molecular vibrations that could take place in typical Raman scattering. But the fundamental vibrations can be summarized in the list below:

- stretching: a change in the length of the bond
- bending: a change in the angle between two bonds
- rocking: a change in angle between a group of atoms and the rest of the molecule
- wagging: a change in the plane between the plane of a group of molecules and the plane of the rest of the molecule
- twisting: a change in the angle between the planes of two groups of atoms
- out-of-plane: the atom moves in and out of the plane of the other atoms

The traditional commercial Raman spectroscopy system uses a continuous wave laser at low intensity. In order to achieve good signal, the sample and microscope

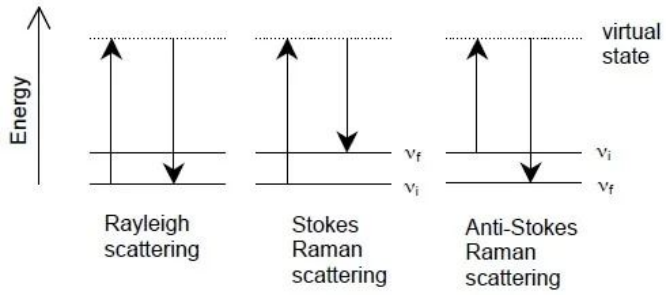

Figure 2. Rayleigh, Stokes Raman and anti-Stokes Raman frequency changes [38].

objective must be kept in isolation from any stray light as it would interfere with the spectra. Recently a novel setup using a pulsed laser coupled with an echelle spectrograph has been proposed by George and Shameem [39, 40]. In our setup, the camera on the echelle spectrograph is gated and the relative intensity of the Raman scattered light, compared to the room, is very high in the timeframe of the pulse duration; hence, special room darkening procedures are not needed to prevent ambient light from interfering [40]. This new approach also shows promise for its ability to allow the coupling of both LIBS and Raman in one experimental setup. Although Raman spectroscopy has been used in recent works to study lithium hydride hydrolysis products to include $LiOH$, LiD, Li_2O, and $LiOH(H_2O)$, the present work explores the application of this approach to lithium compounds for the first time. [9, 10].

2.3 LIBS

Laser induced breakdown spectroscopy has been a method of elemental analysis since 1983 when it was pioneered by Cremer and Radziemski at Los Alamos National Laboratory [41]. In this method, a laser is focused in both time and space onto the sample of interest in order to impart a large energy fluence. This is accomplished using a pulsed laser and optical lenses. When sufficient energy fluence is incident on the sample, the material becomes super-heated and creates a plasma. In this plasma

ions, electrons and dissociated atoms are formed for a short period of time and then recombine and cool. When they cool, the electrons transition to lower energy states and emit characteristic photons in the process. This emitted light is then captured using a gated camera. Understanding the time evolution of the process is paramount to capturing meaningful data. What follows is a description of the laser ablation and optical emission processes. A graphical representation of a typical LIBS setup is displayed in Figure 3.

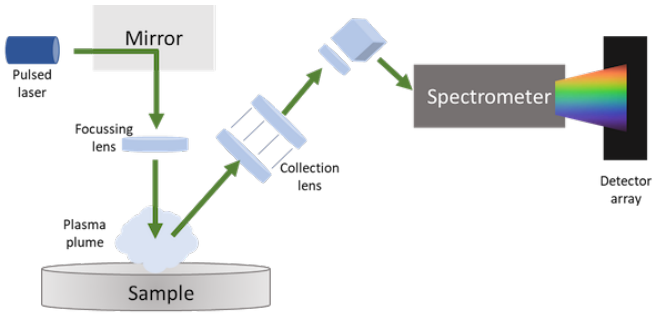

Figure 3. An example of a standard LIBS setup [42].

The spectra observed in LIBS measurements originates from the atoms in the plasma produced by the incoming laser. Emission occurs when a valence electron in a higher energy state returns to a lower energy state and emits a photon with energy equal to the energy difference in the process [43]. Due to the element specific energy level structures, a spectra will consist of discrete lines associated with these energy level transitions. Measurements of intensities of spectral lines from different atoms can be used to determine number densities of those respective elements [41]. The emission lines of interest in this current work are those from lithium, oxygen, hydrogen, and carbon. Though these are the elements of interest, others are sure to be present such as the buffer gas and any potential contaminants in the sample which may originate at the supplier or may be introduced during the sample making process. Each of the atoms have their own energy level scheme. As an example,

Figure 4 displays the energy levels for orbital electrons in neutral lithium and the wavelengths associated with these transitions.

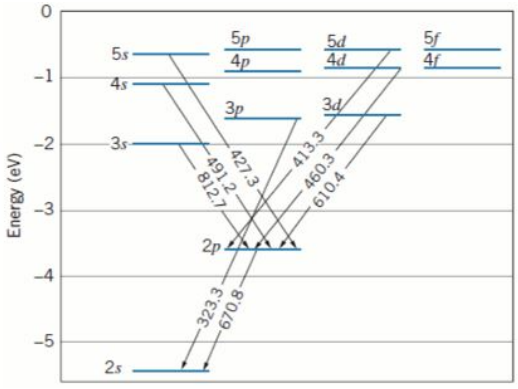

Figure 4. The energy level diagram for lithium [44].

Observation of atomic emission can be traced back as early as the 1500s where the it was noted the color of flames changed with the introduction of different materials, specifically in the smelting of metal ores where the change in flame color indicated when the metal was ready to be cast [43]. Over the years, the use and precision of atomic emission spectra advanced until plasma was used for atomic emission spectroscopy in 1964. In the case of LIBS, the laser induces a plasma when the energy of the pulse is imparted on the sample of interest. This is known as a LIP. The process of forming this LIP also is known as laser ablation.

2.3.1 Laser Ablation

In addition to forming a LIP, ablation also includes the formation of gaseous vapor and fine particles [41]. The light emitted from the plasma is what is observed for LIBS. The ejected particles and gaseous vapor leave behind a crater. Since the crater is very small (microns), LIBS is considered a quasi-nondestructive analysis technique. Understanding the time evolution of this process enables one who is conducting LIBS to understand and optimize the parameters surrounding the technique. The ablation

process is broken into three major steps which are illustrated in Figure 5 and described below.

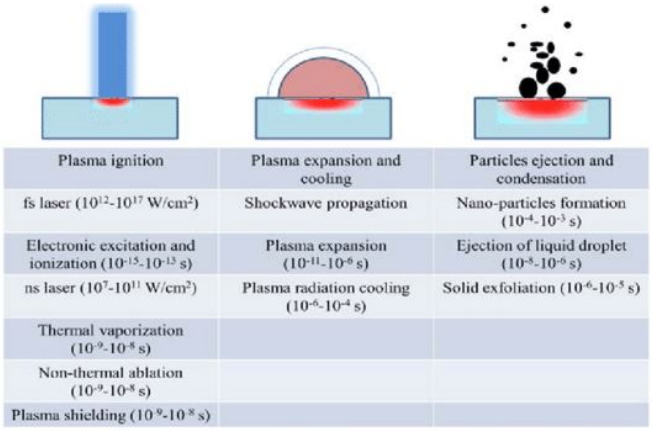

Figure 5. The ablation process broken into three major steps [41].

The first step in laser ablation is the plasma ignition. This is initiated by the coupling, or the deposition, of the laser pulse energy into the sample. For nanosecond lasers, the primary plasma ignition mechanism is thermal [41]. Discussion of the potential advantages and applications of pico- and femtosecond lasers will be addressed in Section 5.1. The temperature of the sample will rise rapidly during the laser pulse to the point of vaporization. That vapor then further absorbs energy from the incoming laser pulse until the atoms become ionized. These super-heated ions and free electrons form a plasma. Several factors impact the coupling of energy into the sample. One such factor is the density of the material; the more dense the material is, the lower the ablation threshold will be [41]. Another factor is the color of the material; a darker material will absorb more energy from the laser pulse than lighter materials. This became an issue which is discussed in Section 3.4.

Second is plasma expansion and cooling. During this stage, the plasma continues to expand after the laser pulse has ended. The plasma expansion occurs on the time period of tens of picoseconds to one microsecond following the laser incident on the

sample, after which the plasma begins radiatively cool. The cooling process lasts from microseconds to tens of milliseconds following the laser incident on the sample. It is during this time that LIBS spectra is acquired for atomic identification. Prior to approximately one microsecond, there is a strong continuum background from the accelerated electrons and ions (Bremsstrahlung process) which dominates the spectra. Understanding these timing considerations is key to acquiring useful information from the current research. The last stage of the ablation process is particle ejection and condensation. This is the step where the ejected materials settle down and the crater is formed.

2.3.2 Depth Profiling

One advantage of LIBS is the ability to provide depth profiling of a sample. Many other optical emission spectroscopy techniques are limited by the mean free path of light in the sample. In order to perform depth profiling with these other methods, a layer of the sample must be removed before analysis at the next depth. But, during a single pulse of LIBS, a small amount of sample is removed and a crater on the scale of microns is formed. The bottom of the crater becomes the new surface for LIBS analysis. This can be repeated until a desired depth is reached. After the crater depth has been characterized, the spectra can be paired with the corresponding depth into the sample to provide a layer by layer analysis [45–47].

2.3.3 Potential Challenges

When an atomic emission line suffers from self-absorption, it will appear as a flat-top on the peak or, in more extreme cases, a dip known as self-reversal. A visual of this effect is shown in Figure 6. This occurs when the plasma is not optically thin. Instead, light emitted from the atoms in the center of the plasma is absorbed by the

cooler atoms of the same element on the peripheral [28]. This phenomena has been observed in lithium hydroxide by Wood in his study of isotopic shifts in lithium [48].

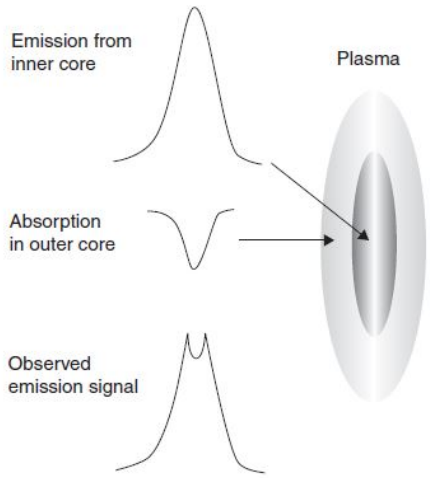

Figure 6. Diagram illustrating the origin of self-absorption [28].

When analytes have emission lines with observable self-absorption, the integrated area under the measured peak is no longer proportional to the species concentration. When possible, atomic emission lines which do not have self-absorption are preferred for analysis. If such lines are not an option, there are techniques for reducing this effect. These include performing LIBS under a purge gas such as helium or under vacuum [28, 49]. Other techniques propose methods to account for self-absorption during post-processing [28].

In order for depth profiling to be successful, the shot to shot variation must be negligible; this is possible if the properties of both the laser and the sample material are held constant. An issue arises when the material at the bottom of the crater is not of the same composition or density as the surface prior to ablation. These changes may occur due to particle deposition following plasma cooling and condensation. Another factor to consider is the thermal propagation into the surrounding material. When the

surrounding material is heated its chemical, molecular, and chromatic properties can change [28, 45]. These changes increase shot to shot variation in LIBS and decrease the resolution of the technique.

2.4 Lithium Spectra

The lithium compounds of interest in this study have been studied by both LIBS [11] and Raman spectroscopy [5, 9, 10, 12–16]. These studies establish the known spectra associated with these techniques and these compounds.

2.4.1 Raman Spectra of Lithium Compounds

The Raman spectra of lithium hydride and its hydrolysis products have been studied thoroughly over the years, establishing a wealth of data for each of the molecular compounds of interest in this study. Raman lines are reported in units of cm^{-1} and are independent of the wavelength of the incident light as long as the incident light is far-off resonance from the excited electronic states. However, for incident light near resonant wavelengths, certain wavelengths tend to perform better. In the case of lithium compounds, it was determined by Stowe that lower wavelengths tend to reduce fluorescence (a common interference in Raman spectra) [9].

The Raman lines of interest in this study will be the Stokes lines, particularly those above 615 cm^{-1}. This cutoff is applied due to the use of a dichroic mirror with cutoff at 550 nm that corresponds to 615 cm^{-1} for 532 nm incident light. Keeping this cutoff in mind, the Raman lines and their corresponding molecular compounds are listed in Table 1 [10, 14, 15].

Table 1. A list of the Raman lines of interest for lithium compounds in this study.

Compound	Raman(cm^{-1})
LiH	825
LiH	1228
LiH	1814
LiH	2087
LiOH	621
LiOH	3665
Li2CO3	1090
Li2CO3	1461

A Raman spectra of LiH as determined by Maupoix et al. [13] is displayed in Figure 7. Figure 8 shows an example spectra of $LiOH$ as measured by Gorelik et al. [10]. Finally, Figure 9 is a Raman spectra of Li_2CO_3 as measured by Brooker and Wang [15].

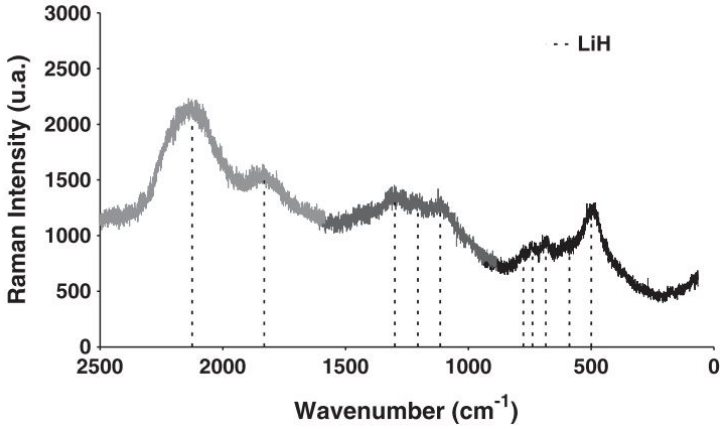

Figure 7. Raman spectra of LiH as obtained by Maupoix et al. in a study on the grain-size dependence of the hydrolysis of LiH [13].

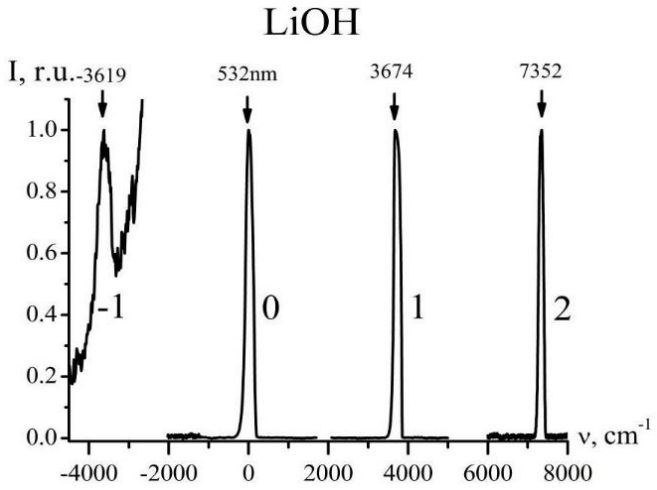

Figure 8. Raman spectra of $LiOH$ as obtained by Gorelik et al. [10].

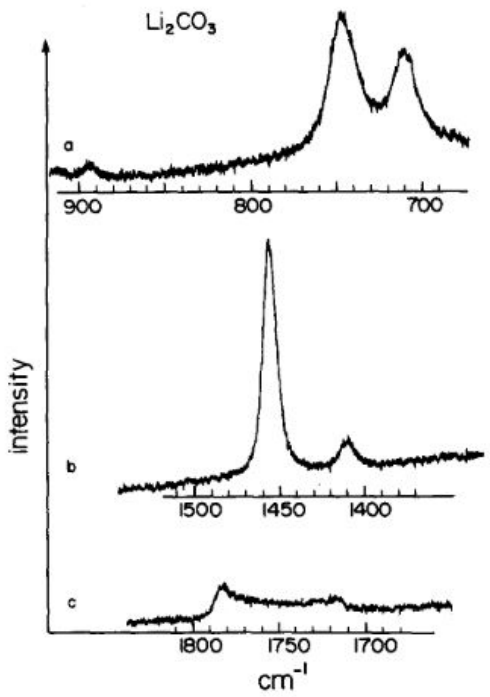

Figure 9. Raman spectra of Li_2CO_3 as obtained by Brooker and Wang [15].

2.4.2 LIBS Spectra of Lithium Compounds

As described previously, LIBS is an atomic emission spectroscopy technique. Thus, the optical emissions under observation are those from the elements of interest. Again, the lithium compounds of interest are LiH, $LiOH$, and Li_2CO_3. Li_2O is also of interest but was not evaluated in this study. Given these compounds and the dry buffer gas used for safe handling of lithium hydride, the elements of primary focus are lithium, hydrogen, oxygen, carbon, and nitrogen. Table 2 displays the primary atomic lines of interest and the elements to which they correspond. Data for selection and identification of these lines was obtained from the NIST LIBS Database [50].

A simulated spectra, assuming no self-absorption can be acquired from the NIST LIBS Database. Choosing a mixture of 50% LiH, 25% $LiOH$, and 25% Li_2CO_3 in an atmosphere of nitrogen would produce a spectra approximated by Figure 10.

From this simulated spectra, one can observe the carbon line at 833 nm is negligible in comparison to the other lines. Special treatment may be required to view this atomic line. Carbon has much stronger emission peaks at 247.8 nm and 909.4 nm but these are outside the viewable range of the spectrometer in use for this study. Though atomic emission lines from carbon may not be visible, the ratios of the other peaks may still offer the chemical information about the lithium compounds present. This will be further addressed in the section on chemometrics.

In a study conducted at Y-12 Security Complex, Ponzio et al. were able to use LIBS to observe the ingrowth of the oxygen atomic line at 777 nm as evidence of oxidation on the surface of LiH samples [11]. A similar method can be used in the present study to observe the increased presence of oxygen and changing ratios of lithium and hydrogen in various mixtures.

Table 2. List of elements and their primary atomic lines of interest.

Element	Wavelength (nm)	Transition (conf./term/J)
Li	610.354	$1s^2 3d/^2D/\frac{3}{2} \longrightarrow 1s^2 2p/^2p^o/\frac{1}{2}$
	610.365	$1s^2 3d/^2D/\frac{3}{2} \longrightarrow 1s^2 2p/^2p^o/\frac{3}{2}$
Li	670.776	$1s^2 2p/^2p^o/\frac{3}{2} \longrightarrow 1s^2 2s/^2S/\frac{1}{2}$
	670.791	$1s^2 2p/^2p^o/\frac{1}{2} \longrightarrow 1s^2 2s/^2S/\frac{1}{2}$
Li	812.623	$1s^2 3s/^2S/\frac{1}{2} \longrightarrow 1s^2 2p/^2p^o/\frac{1}{2}$
	812.645	$1s^2 3s/^2S/\frac{1}{2} \longrightarrow 1s^2 2p/^2p^o/\frac{3}{2}$
H	656.271	$3d/^2D/\frac{3}{2} \longrightarrow 2p/^2p^o/\frac{1}{2}$
	656.272	$3p/^2p^o/\frac{3}{2} \longrightarrow 2s/^2S/\frac{1}{2}$
	656.277	$3p/^2p^o/\frac{1}{2} \longrightarrow 2s/^2S/\frac{1}{2}$
	656.285	$3d/^2D/\frac{5}{2} \longrightarrow 2p/^2p^o/\frac{3}{2}$
O	777.194	$2s^2 2p^3(^4S^o)3p/^5p/3 \longrightarrow 2s^2 2p^3(^4S^o)3s/^5S^o/2$
	777.417	$2s^2 2p^3(^4S^o)3p/^5p/2 \longrightarrow 2s^2 2p^3(^4S^o)3s/^5S^o/2$
	777.539	$2s^2 2p^3(^4S^o)3p/^5p/1 \longrightarrow 2s^2 2p^3(^4S^o)3s/^5S^o/2$
C	833.514	$2s^2 2p3p/^1S/0 \longrightarrow 2s^2 2p3s/^1p^o/1$
N	742.364	$2s^2 2p^2(^3P)3p/^4S^o/\frac{3}{2} \longrightarrow 2s^2 2p^2(^3P)3s/^4p/\frac{1}{2}$
N	744.229	$2s^2 2p^2(^3P)3p/^4S^o/\frac{3}{2} \longrightarrow 2s^2 2p^2(^3P)3p/^4p/\frac{3}{2}$
N	746.831	$2s^2 2p^2(^3P)3p/^4S^o/\frac{3}{2} \longrightarrow 2s^2 2p^2(^3P)3s/^4p/\frac{5}{2}$
N	818.487	$2s^2 2p^2(^3P)3p/^4p^o/\frac{5}{2} \longrightarrow 2s^2 2p^2(^3P)3s/^4p/\frac{3}{2}$
	818.802	$2s^2 2p^2(^3P)3p/^4p^o/\frac{3}{2} \longrightarrow 2s^2 2p^2(^3P)3s/^4p/\frac{1}{2}$
N	821.634	$2s^2 2p^2(^3P)3p/^4p^o/\frac{5}{2} \longrightarrow 2s^2 2p^2(^3P)3s/^4p/\frac{5}{2}$
N	824.239	$2s^2 2p^2(^3P)3p/^4p^o/\frac{3}{2} \longrightarrow 2s^2 2p^2(^3P)3s/^4p/\frac{5}{2}$

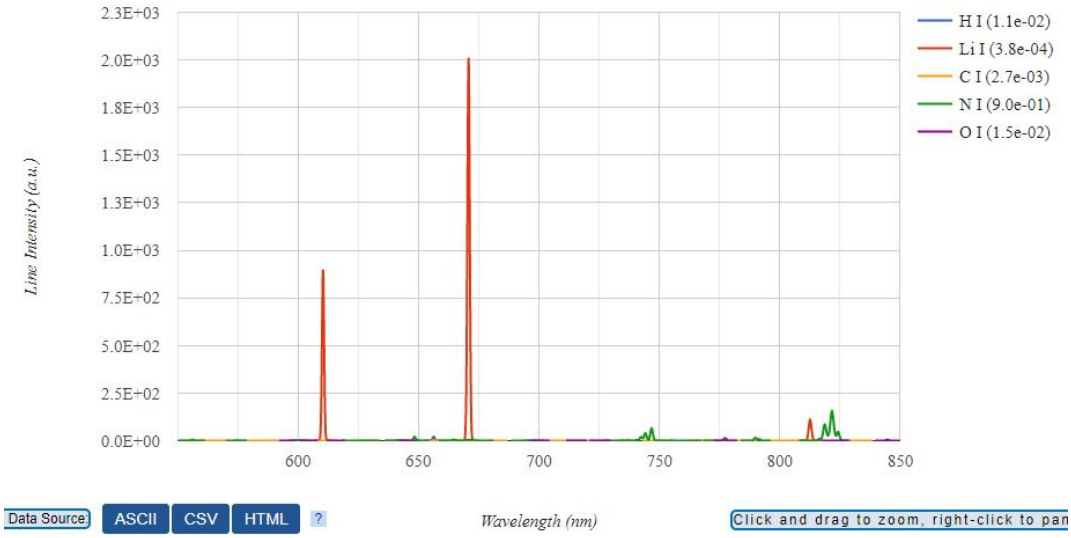

Figure 10. Simulated LIBS spectra approximating a 50/25/25 mixture of $LiH, LiOH, \& Li_2CO_3$ in a nitrogen atmosphere [50].

2.5 Data Fusion

Because this research conducted both LIBS and Raman measurements, the data set lends itself to data fusion. Data fusion is when multiple data types are used together to create a more accurate model [51]. Although there are several categories of data fusion which are used to describe what level the data are fused together, this research uses low-level data fusion because the raw data from each method is fused together prior to any manipulation or characteristics extraction [51]. LIBS and Raman spectroscopy are often used together due to their complimentary nature. Both are spectroscopic measurements and they provide complimentary information about the sample. LIBS provides elemental composition information and Raman provides molecular identification. Data fusion of LIBS and Raman spectra is increasing in popularity with several publications within the last year demonstrating its application to terrestrial and martian environmental samples [52–54]. Each of the cited works

paired LIBS-Raman data fusion with chemometrics techniques to identify the presence of minerals and other naturally occurring elements of interest.

2.6 Univariate Regressions

When regressions on spectral data are being modeled where the differentiating components in the spectra are limited to a single or perhaps two emission lines, a ratio of emission line intensities can be used to model the relationship. This is a very simple and effective technique when the features under consideration are few. The ratio of peaks is a standard technique for determining percent concentration of an element [28, 41]. Recently, Rao demonstrated the efficacy of this technique when modeling percent concentration of gallium in cerium samples using the ratio of a single gallium peak to a single cerium peak [55].

2.7 Chemometrics

Chemometrics, as used in this study, is"the chemical discipline that uses mathematical and statistical methods to provide maximum chemical information by analyzing chemical data" [23]. Chemometrics has been used on LIBS data in recent years by Stipe and others. Stipe used PLSR to quantify chromium, nickel, and manganese in steel alloys in 2010 [26]. Zhang reviews uses of chemometrics on LIBS data during the five year window from 2012 to 2016 [25]. The advantage of multivariate chemometrics is the robustness of the predictive models it produces when compared to univariate analysis as described in Section 2.6. Zhang notes the fragility of using univariate methods for creating calibration curves due to the susceptibility to fluctuations in laser energy and matrix effects in the sample [25]. Further, recent works within the last year have employed chemometrics with data fusion to further enhance predictive capability [52–54]. Of note is the work NASA is doing using chemometrics

and data fusion on the Mars rover and other solar system exploration modules [53]. The two methods described below are employed due to their popularity and accepted use in LIBS and Raman communities. The intent is to demonstrate their use for creating a calibration curve or predictive model for determining various concentrations of lithium compounds in a bulk lithium sample.

2.7.1 Principal Components Regression (PCR)

Principal components regression takes the output of a principal components analysis (PCA) and performs regression analysis on those principal components (PCs) [56]. PCA is a method of reducing the dimensionality of a data set by finding/creating latent variables which explain the bulk of the variance in the data set. The advantage to using PCs for regression analysis is they allow for the reduction of multicollinearity [57]. Multicollinearity occurs when multiple explanatory variables correlate with each other [58]. By selecting only the PCs which explain the bulk of the variance, multicollinearity can be minimized. This is advantageous because multicollinearity is known to lead to unstable and unreliable estimates of regression coefficients [58].

Choosing which PCs to use can be performed by using one of a few rules of thumb. The first one is to decide how much variance must be explained by a PC in order to be included (e.g. 10%). If a PC fails to explain at least the determined level of the total variance, then it is not included in the regression model. The other is to decide how much total variance must be explained (e.g. 90%). In this case, each PC is included until 90% of the variance has been explained beginning with the PC which explains the highest portion of the variance and then working down from there. Figure 11 shows a graphical example of this decision process with purely theoretical data. Once the PCs have been chosen, a linear least squares fit is performed using them to create the regression model for the data set. Recent work has used PCR separately with

both LIBS and Raman data and in data fusion [48, 52, 55].

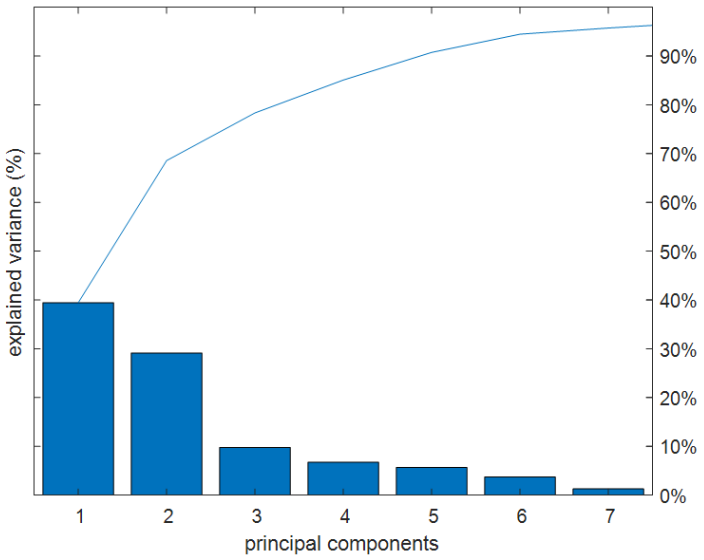

Figure 11. Scree plot of variance explained per principal component (bar chart) and total variance explained by sum of principal components (line plot). To be used in deciding how many principal components to use in analysis (theoretical data for conceptual purposes) [59].

2.7.2 Partial Least Squares Regression (PLSR)

One drawback to using PCR is the dependent variable (in the case of this study it is the lithium compound percent concentration) is not considered when constructing the PCs. For this reason, there is risk the PCs will be able to accurately account for the variance in the predictors without being able to accurately predict the response variable. This is the consequence of using an unsupervised technique [60].

On the other hand, PLSR is a supervised learning technique with many similarities to PCR. PLSR, like PCR, also reduces the dimensionality of the data by finding latent variables within the entire set of variables. It identifies a new set of features from the data which are linear combinations of the original variables. Unlike PCR, however, PLSR uses the response variable to inform the selection and weighting of

these new variables [60]. This is accomplished by minimizing the covariance between the predictors and the responses [61].

PLSR has become very popular in chemometrics [48,52–55]. However, when compared with PCR, the advantages are often not apparent since there is a trade-off. Even as the supervised technique of PLSR reduces bias amongst the variables, it can also suffer from overfitting. Thus the gains over PCR can be moot, suggesting one technique is not more useful than the other across all applications [60]. A comparison must be made to determine which technique performs better for the dataset at hand.

The same method surrounding the discussion on Figure 11 will be used when deciding how many factors to include in the PLSR model. Namely, take the number of factors corresponding to a chosen cutoff for total variance explained in the predicted variable or a cutoff for variance explained per additional factor included in the model.

III. Methodology

This experiment's methodology was divided into four sequential stages: sample selection and preparation, Raman measurements, LIBS measurements, and data processing. It is important for the Raman measurements to be taken prior to the LIBS measurements due to the fact the measurements were conducted on the same samples for both methods. Raman spectroscopy must be conducted before LIBS because it is a completely non-destructive technique and will not alter the results obtained from LIBS. The reverse is not true.

3.1 Sample Selection and Preparation

The samples chosen for this study were chosen based on goals of an ongoing research study on the hydrolysis and carbonation of lithium hydride. The reactions detailed in Eqs 1-4 in Section I outline the lithium compounds of interest and how they are formed. The present study focuses solely on the reactions in Eqs 1 and 4 and does not consider the role of Li_2O. Another compound not included is lithium hydroxide (monohydrate) which results from $LiOH$ being exposed to moisture in the air. The study of these two additional compounds is beyond this scope.

Pure samples of LiH, $LiOH$, and Li_2CO_3 were initially created to establish that the techniques will indeed measure the intended compounds of study in the simplest of cases. Then various mixtures were created, pairing two compounds together in multiple concentrations. The pairing was based on Eqs 1 and 4. LiH was paired with $LiOH$ in concentrations representative of $LiOH$ ingrowth in a LiH sample. $LiOH$ was paired with Li_2CO_3 in concentrations representative of lithium carbonate growing into lithium hydroxide. Two additional samples were created and analyzed: one with all three compounds and one with carbonate mixed with hydride. Table

(3) outlines the sample composition matrix. The uncertainty is less than 1% for all concentration values in the table. In order to avoid/minimize cross-contamination, all equipment involved in sample preparation was thoroughly cleaned after each sample set was prepared.

Table 3. Concentration of Lithium Compounds in Samples of this Study

Label	LiH [%]	$LiOH$ [%]	Li_2CO_3 [%]	Quantity
LiH	100	0	0	4
LiOH	0	100	0	4
Li2CO3	0	0	100	1
Mix1	90	10	0	3
Mix2	75	25	0	4
Mix3	50	50	0	4
Mix4	0	83	17	4
Mix5	0	70	30	4
Mix6	0	50	50	4
Mix7	50	25	25	4
Mix8	75	0	25	4

3.1.1 Pellet Pressing Procedure

The lithium compounds were acquired from Sigma-Aldrich in powdered form. This enables mixing and tuning of sample preparation such as size, pressure, etc. LiH reacts violently with moisture and therefore must be handled in a "dry" environment [30]. While the humidity level for this "dry" environment is not defined, Sifuentes showed that relative humidity of 1% has led to very low mass increase in LiH samples [12].

Liquid nitrogen boil-off was used to purge a glove box and create a dry environment for handling the samples. The purity of the nitrogen is unknown. The samples were placed in an air-tight cell with a viewport in order to allow analysis of the samples while maintaining the dry environment. The view port allowed the laser to interact with the sample and allowed for light collection without ever exposing the sample to

the ambient conditions of the lab. Purging the sample atmosphere with nitrogen not only minimized the presence of moisture but also minimized the presence of other constituents of ambient air, including CO_2. The use of nitrogen as opposed to other purge gases is rooted in the fact that it is the most common purge gas for LiH handling and storage. It is also the most widely available purge gas on the market. Other buffer gases such as helium and argon have been shown to improve LIBS spectra and would have likely improved the LIBS measurements in this study [11, 62, 63]. Their use is mentioned in the Future Work subsection of the Conclusion of this paper. The use of nitrogen also poses potential issues where LiH is heated above 200^{o}C such as the periphery of a plasma where material may react with the gas to form nitrogenous compounds [18]. This is discussed later in greater detail.

The equipment used in the glove box consisted of a lab scale with 1 mg precision, a mortar and pestle, a powder sample mixer, and a pellet press. Due to the space constraints of the glove box, each piece of equipment was chosen based on their size to allow for maneuvering in sample preparation. The trade-off for space in this instance was most notably the precision of the scale, the size of the sample pellets, and the maximum pressure of the press. However, the scale's precision was acceptable because the mass of each lithium compound in the mixtures was at least 100x the precision of the scale so as to reduce the percent uncertainty in the measurement below 1%.

The mixed powders were ground with a mortar and pestle prior to pressing to ensure uniform particle size. Lal et al. demonstrated the utility of grinding powder samples prior to pressing in their study on optimization of pellet pressing parameters for use in LIBS [64]. The advantage of this was also confirmed in an unpublished study conducted on $LiOH(H_2O)$ previously. This study can be found in Appendix A. After grinding, pure samples were placed into containers with mixing balls and mixed in a Fluxana MUK mixer to ensure homogeneity. Following mixing, the powder

was transferred in small quantities into the press die. The die is 7 mm in diameter and produces, on average, a pellet 1.5 mm in thickness. The pellet press is a Specac mini pellet press with maximum pressure of 2 tons. The pellets were pressed to 1.5 tons and this pressure was sustained for 3 min. During those 3 min the pressure was iteratively adjusted such that the pressure was maintained at 1.5 tons. By the end of the 3 min, settling had subsided and the pressure was holding constant. The decision to use 1.5 tons was also based in the study referred to in Appendix A. For samples which were a mix, rather than purely a single compound, the compounds were weighed on the laboratory scale and the desired ratio was determined by percent mass. This step was accomplished following grinding and prior to mixing. The rest of the sample making steps for the mixtures followed those above. Figure 12 shows the glove box layout and equipment as used in this study.

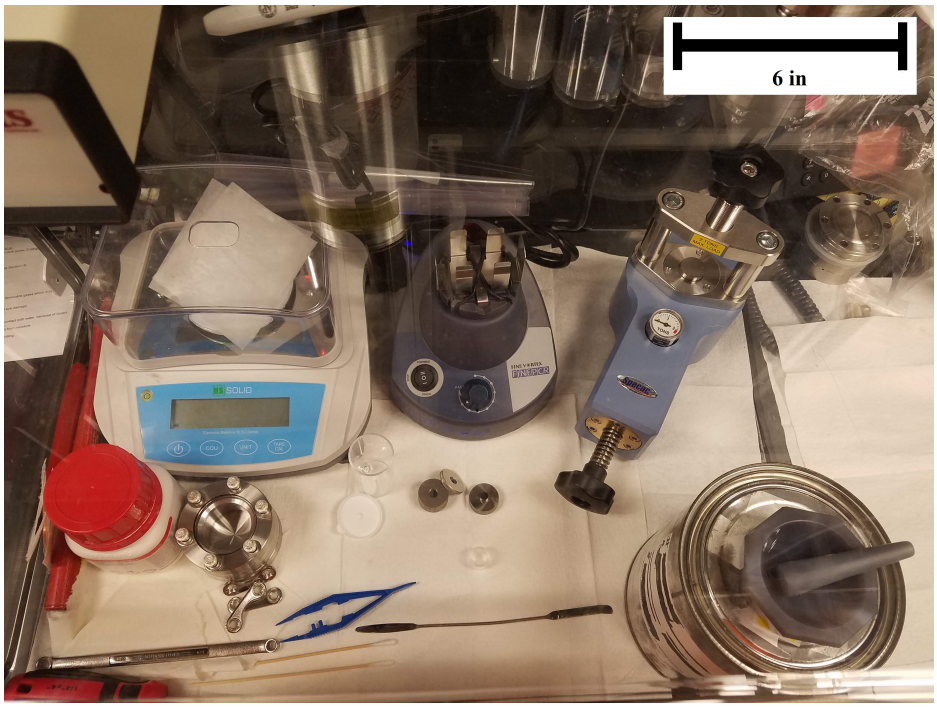

Figure 12. The glove box and equipment for creating samples prior to pressing a batch of pellets containing LiH and $LiOH$.

After samples were pressed, they were affixed to the bottom of the conflat flange cell using a thin layer of vacuum grease. This served to keep the samples from shifting in the cell while maneuvering the equipment. During LIBS, the grease also kept the samples from shifting during the ablation process. This was a concern after LIBS experiments on similar samples caused them to shift, sometimes dramatically, during the study described in Appendix A. One particular issue was encountered while pressing and affixing pure Li_2CO_3. The pellet was particularly brittle and would split when removing from the die. Figure 13 shows a pure lithium carbonate pellet broken after removing from the die. To remedy this, the pure Li_2CO_3 was left in the

Figure 13. The pure Li_2CO_3 pellet which broke upon removal from the pellet press die on which it is sitting in this figure.

die for analysis. Other samples did not experience this issue as LiH and $LiOH$ can bind into pellets without the use of a binder even when mixed with the carbonate in the mix samples. A batch of samples is shown in the conflat flange cell in Figure 14.

During the sample making process the humidity was monitored using a humidity probe (electro-tech systems model 554) and digital display (electro-tech systems model 5100-240). Humidity levels for all batches of samples varied from 1.1% to 1.7%. Due to the need for opening the box for sample removal and cleaning between batches, the starting humidity level varied from day to day. This, along with time constraints (not being able to purge several days for each batch), explains the variance in this

Figure 14. Conflat flange sample cell with UV fused silica viewport. The spacer is used to extend the distance between the focal point of the laser and the glass to avoid damage to the viewport.

parameter. The ability to conduct analysis immediately following sample preparation minimizes the potential impacts to the sample integrity.

3.2 Dual Setup

The use of a single setup for conducting both LIBS and Raman has an obvious advantage of saving time and streamlining the sample analysis process. Shameem et al. demonstrated the versatility of the echelle spectrograph for use in both LIBS and Raman spectroscopy using a single setup. The only two changes from LIBS to Raman is the reduction of the energy fluence in order to prevent ablation during Raman measurements and timing the Raman observation window to match the signal arrival time at the detector [40]. This was accomplished using a de-focusing lens, by reducing the laser power, and adjusting the timing of the detector.

This study employed a Quantel Nd:YAG pulsed laser operating at 532 nm with a 10 ns pulse width. A Berkeley Nucleonics digital delay generator, Model 577, was used as a trigger source for both the laser and the camera on the spectrograph. The laser pulse is directed through a polarizer followed by a polarizing beamsplitter. This allows for power tuning without adjusting the laser trigger settings. For the Raman measurements, the light is directed through a de-focusing lens that is set twice the

focal length from the dichroic mirror to avoid focusing the laser onto the mirror and ablating the surface. The dichroic mirror has a cutoff wavelength of 550 nm, below which light is reflected and above which light is transmitted. The laser is then directed through the final focusing lens and onto the sample through the viewport on the conflat flange cell.

The light from the sample radiates outward in all directions, thus it is diverging and must be collimated before begin focused into the optical fiber which then channels the light to the spectrograph. The light which is incident upon the final focusing lens accomplishes this collimation. Light above the cutoff of the dichroic mirror is transmitted through the notch filters and into the light collection optics for the optical fiber. There are two notch filters, one is OD-4 and the second is OD-6. Together they provide light rejection equivalent to OD-10 for any laser light which made it through the dichroic mirror. For LIBS measurements, the defocusing lens is simply rotated out of the way and all other equipment remains the same. A schematic diagram of the setup for this study is shown in Figure 15.

3.2.1 Echelle Spectrograph for Raman and LIBS

An echelle spectrograph differs in comparison to a standard monochromater in that it uses 2-D diffraction rather than 1-D diffraction and it has a much broader bandwidth. If one desires to view multiple lines which are not within the small bandwidth of a Czerny-Turner style monochromater, one would need to take an image on the camera at one position on the spectrum, adjust the gratings to another position and take another spectra. This requires multiple exposures and in LIBS this means separate ablations. With an echelle spectrograph, the bandwidth is hundreds of nanometers. In particular, the echelle spectrograph used in this present work was a Catalina Scientific EMU-120/65 model which allows the user to take an exposure and

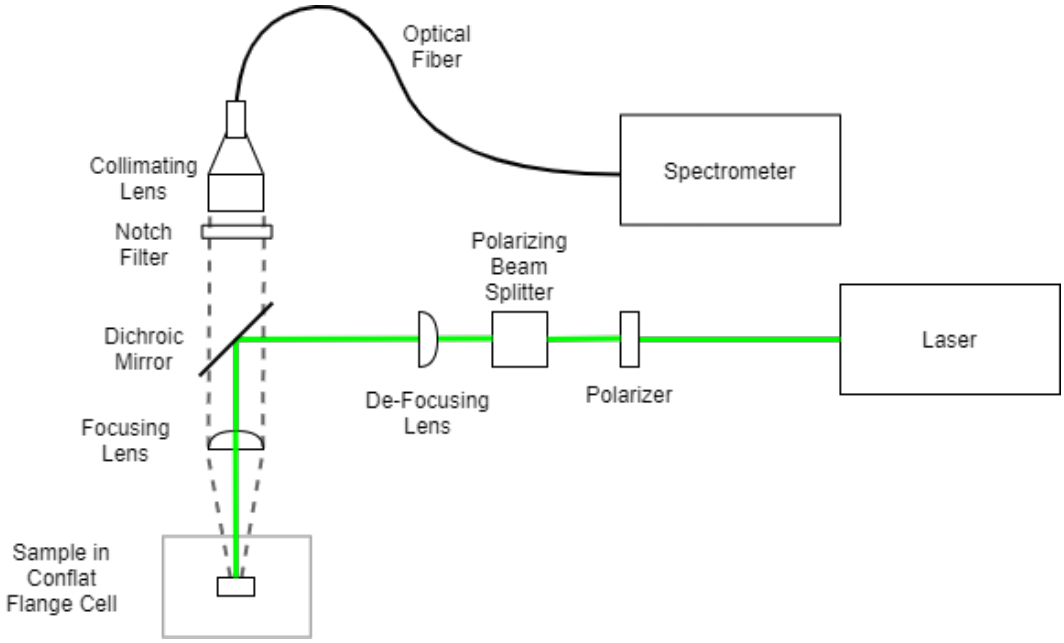

Figure 15. The dual purpose setup used for both LIBS and Raman spectroscopy.

observe light from 325 nm to 925 nm.

This broad bandwidth is especially useful in chemometrics with LIBS data because at least some spectral lines from nearly every element are present in this range making it possible to collect data from every element of interest in a single spectra. The same benefit is true for conducting Raman spectroscopy, as long as the excitation laser wavelength is below approximately 700 nm. This is because the Raman signal is shifted from the excitation wavelength. If the wavelength of the excitation source is too close to the end of the operating range of the spectrograph then the Raman shift will not be observed. In this study, the largest Raman shift is approximately 3600 cm^{-1} ($LiOH$), the laser wavelength is 532 nm placing a shift of 3600 cm^{-1} around 658 nm, so this works very well.

The spectrograph was calibrated for wavelength twice daily using a Hg/Ar calibration lamp. The first calibration was performed in the morning prior to beginning measurements. The second calibration was performed half-way through the day.

Along with the wavelength calibration, an order optimization and flat-field calibration was also performed. The order optimization uses an image of a continuum light source (deuterium halogen) to inform the optimization of the cutoff between orders using an internal algorithm in KestrelSpec. KestrelSpec is the data acquisition and analysis software from Catalina Scientific which accompanies the spectrograph. An image of a deuterium/tungsten and halogen lamp is displayed in Figure 16. In addition to order optimization, a flat-field calibration is performed using the halogen lamp to approximate a black body radiator.

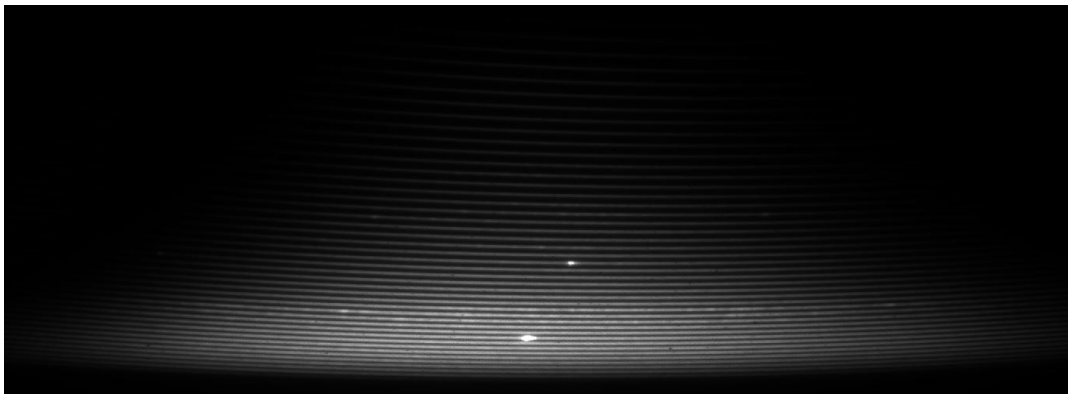

Figure 16. Image of a deuterium/tungsten and halogen lamp taken with the echelle spectrograph.

3.3 Raman

As mentioned above, Raman measurements were taken prior to LIBS. Due to the spot size of the laser at the sample and the field of view of the light collection optics, spectra were taken from five positions on each of the samples. The numbering and flow of the positions on each sample and the order of the samples analyzed is illustrated in Figure 17.

The Raman spectra were acquired via integrating images in a single exposure and then accumulating multiple exposures to form the final image. This was done at

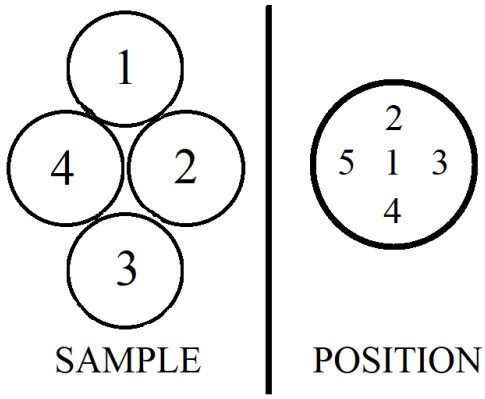

Figure 17. Sample and position numbering as used in Raman measurements.

a repetition rate of 10 Hz for 600 pulses per exposure with 5 exposures. The gate delay and gate width of the ICCD camera were optimized for capturing the scattered light. The exposure time, which is how long the camera shutter is open, is set to its minimum value (1 ms). Microchannel plate (MCP) gain is adjustable from 0-4000 on a non-linear scale. The settings for the Raman measurements can be found in Table (4).

Table 4. Equipment parameters for Raman measurements.

Equipment	Parameter	Value	Sync
Laser	Flashlamp Trigger	0 μs	T0
	Q-Switch Trigger	250 μs	T0
	Repetition Rate	10 Hz	N/A
	Pulse Width (FWHM)	17.8 ± 0.1 ns	N/A
ICCD	Camera Trigger	0 μs	Q-Switch Trigger
	Exposure Time	1 ms	Camera Trigger
	Gate Delay	140 ns	Camera Trigger
	Gate Width	40 ns	Camera Trigger
	MCP Gain	2500	N/A

In measuring the pure samples a clear distinction became apparent between them. In a single plot, the Raman spectra of the pure samples from 400 cm^{-1} to 3800 cm^{-1} is displayed (See Figure 18). To better view the signal from the pure LiH sample,

the spectra has been zoomed in to 400 cm^{-1} - 2380 cm^{-1} and is shown in Figure 19.

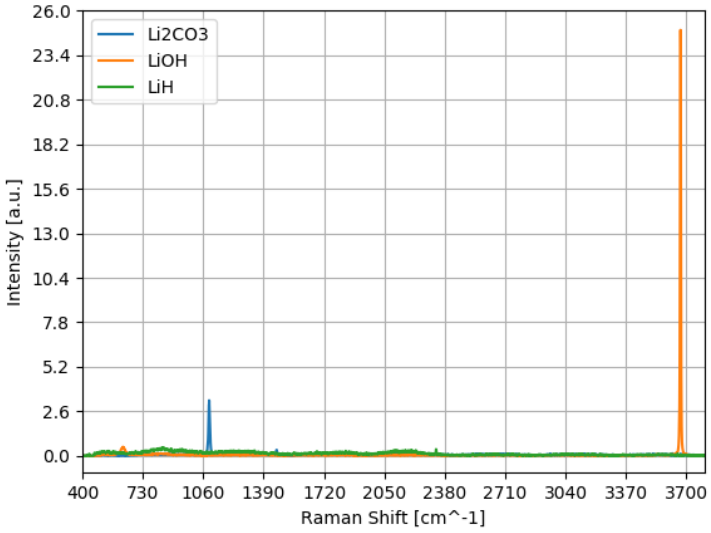

Figure 18. A single Raman spectra from each of three pure samples shows good distinction between the lithium compounds, though LiH is faintly visible on this scale.

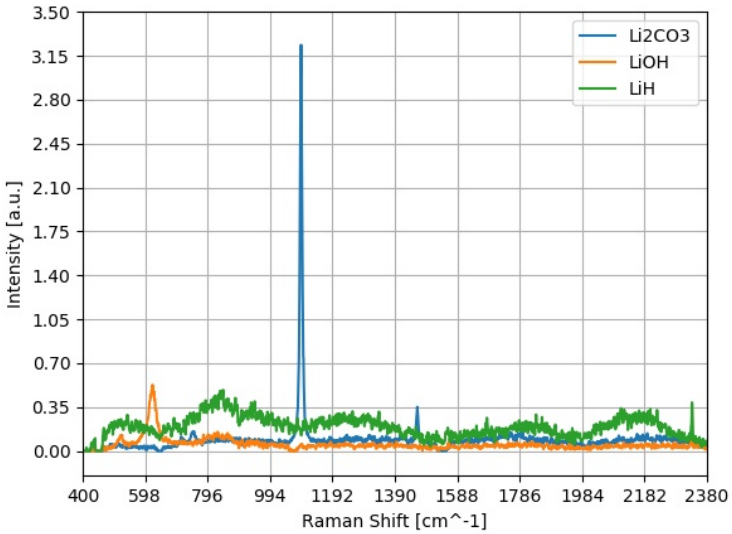

Figure 19. This zoomed-in Raman spectra allows for qualitative confirmation of the LiH Raman signal.

3.4 LIBS

Following Raman measurements, LIBS measurements were taken. The order and flow of samples followed the same order and flow illustrated in Figure 17. The order and flow of positions on those samples, unlike Raman, was based on the ablation crater left by each set of LIBS measurements. An unperturbed position was chosen for the beginning of each set of shots. Each set of shots consisted of 20 ablations in a single position. Each ablation was recorded individually and not integrated or accumulated on camera like the Raman spectra. Each sample was ablated in 10 separate positions for a total of 200 spectra per sample. The purpose for multiple ablations in a single position is to determine the efficacy of the method for depth profiling.

The timing of LIBS measurements differs in comparison to those associated Raman. Where Raman is a scattering process with nearly zero delay on the scale of nanoseconds, the mechanisms of breakdown and recombination which generate the LIBS signal take microseconds to occur. The LIBS parameters for this study can be found in Table (5).

Table 5. Equipment parameters for LIBS measurements.

Equipment	Parameter	Value	Sync
Laser	Flashlamp Trigger	0 μs	T0
	Q-Switch Trigger	190 μs	T0
	Pulse Width (FWHM)	10.7 ± 0.2 ns	N/A
ICCD	Camera Trigger	0 μs	Q-Switch Trigger
	Exposure Time	1 ms	Camera Trigger
	Gate Delay	1.5 μs	Camera Trigger
	Gate Width	6 μs	Camera Trigger
	MCP Gain	1500	N/A

As an example, one of the raw data LIBS spectra for LiH is displayed in Figure 20. As expected, there are no atomic lines for carbon or oxygen in this spectra.

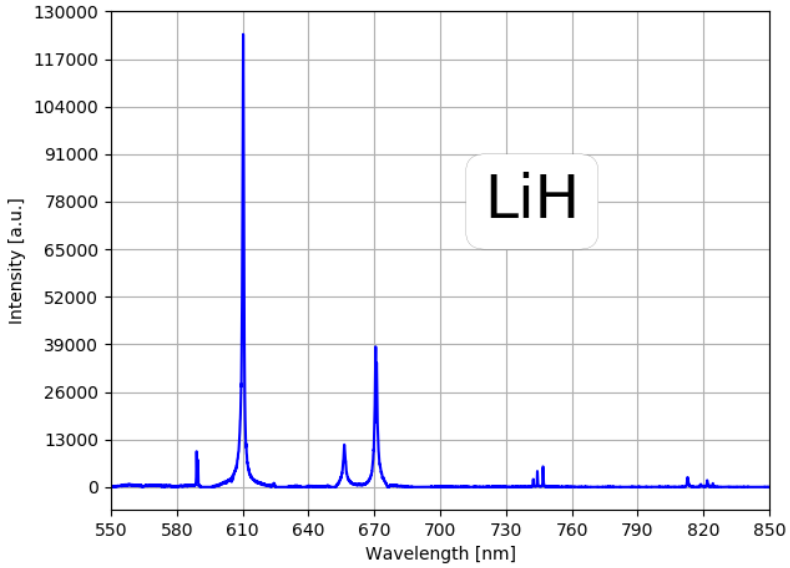

Figure 20. This is a single-shot spectra of pure LiH over the bandwidth captured for LIBS measurements.

3.4.1 Depth Profiling

The study attempted depth profiling on each sample using LIBS. 20 ablations per position were collected. On real-world samples, the intention would be to detect the extent of the hydrolysis and carbonation processes. These processes begin at the sample surface and diffuse inward. Each successive ablation can be paired with the spectra to determine how far $LiOH$ or Li_2CO_3 has grown into the LiH sample.

The depth associated with LIBS measurements can be determined either by taking a depth measurement after every ablation (very time consuming and not always possible) or by taking the depth of the crater after the series of ablations has been accomplished and then simply dividing the depth by the number of shots to get the average depth per shot. The second method requires assumptions about the repeatability and shot-to-shot variations. Taking the average depth assumes the parameters of the laser pulse are constant (pulse energy, spot size, and pulse duration). It also

assumes the parameters of the mass ablated are constant (density, chemical composition, color). These assumptions must hold true and should be assessed for validity before applying the average depth technique.

Crater measurements were taken using a Zeiss Laser Scanning Microscope (LSM). The dimensions of 10 craters were taken to include X-, Y-, and Z-directions. Five craters from each of two $LiOH$ samples were chosen for these measurements. Each crater was created using the same number of ablations (20x). This study assumes these measurements are representative of the other samples since measuring craters from each sample was not feasible. For example, LiH craters could not be measured on the LSM system due to chemical safety protocols since the LSM requires the sample to be sitting in open air with no obstructions between the probing laser and the sample.

3.5 Data Processing

3.5.1 Raman-LIBS Data Fusion

Data fusion was completed on the data obtained from LIBS and Raman measurements. Since there were only five Raman spectra taken from each sample, only the first shot from the first five positions of the LIBS analysis on each sample were used. Prior to fusion, each spectra was normalized by the max intensity of the spectra. This prevented features of one spectra from becoming overly weighted compared to the other due to differing intensity scales. Once normalized, a single Raman spectra was appended to the end of a corresponding single LIBS spectra from the same exact pellet. This created several pseudo-spectra representing each sample. The x-axis of the pseudo-spectra was set to integer values ranging from zero to the length of the data array of the new spectra. With these data fused spectra, the same multivariate analysis techniques were performed as were used on the un-fused data sets.

3.5.2 Univariate and Multivariate Analysis

Univariate analysis was conducted on the LIBS and Raman data. For LIBS this univariate analysis was performed by fitting a linear model between the percent concentration of the ingrowing compound and the ratio of the area under the oxygen peak to the area under the hydrogen peak, 777 nm and 656 nm respectively. This ratio (oxygen/hydrogen) was used in both ingrowth models. These two ingrowth models are (1) $LiOH$ on LiH, and (2) Li_2CO_3 on $LiOH$. The univariate analysis for Raman involved simply taking the ratio of the area under the most intense peak from each compound's signature. For the first regression, the ratio was between the $LiOH$ Raman line at 3665 cm^{-1} and the somewhat continuum of LiH in the region $460 - 2400$ cm^{-1}. In total, four univariate models were created.

In multivariate analysis, PCR and PLS regression were conducted. These models were performed on the two regression sets mentioned above. Raman, LIBS, and LIBS-Raman fused data were analyzed and compared. In total, ten multivariate models were constructed. The metric for effectiveness of the models was both the R^2 value and the Root Mean Square Error (RMSE) value. The R^2 value is a measure of goodness of fit between a regression line and the data it is being fit to and is given by Eqn 5 where RSS is the Residual Sum of Squares and TSS is Total Sum of Squares. The smaller the residuals, the closer the R^2 value is to 1.

$$R^2 = 1 - \frac{RSS}{TSS} \tag{5}$$

The RMSE is a representation of the difference between the observed and the predicted values. More specifically, RMSE is the standard deviation of the residuals of a model and can be described by Eqn 6. Better performance of the model is indicated

by higher R^2 and lower RMSE.

$$RMSE = \sqrt{\frac{\sum_{i=1}^{N}(x_i - \hat{x}_i)^2}{N}} \tag{6}$$

Principle components analysis (PCA) was also performed on the pure samples (LiH, $LiOH$, and Li_2CO_3). The intention was to establish good separation exists between the pure samples in the principal component space. If separation is not observed the likelihood of success for fitting an accurate regression appears bleak. Additionally, PCA was performed on Mix7 and Mix8, though they do not represent a sample composition in one of the above mentioned regressions.

IV. Results and Analysis

This section presents the results of univariate and multivariate regressions for the regressions of interest: $LiOH$ on LiH and Li_2CO_3 on $LiOH$. Multivariate classification is presented for the pure samples as well as Mix7 and Mix8 to establish if distinction of compounds is possible. The following definitions apply for the regressions modeled:

- Regression 1 (R1): represents the ingrowth of $LiOH$ in LiH and is composed of sample batches LiH, Mix1, Mix2, Mix3, and LiOH (in that order).
- Regression 2 (R2): represents the ingrowth of Li_2CO_3 in $LiOH$ and is composed of sample batches LiOH, Mix4, Mix5, Mix6, and Li2CO3 (in that order).

Each of the multivariate analysis techniques (PCR and PLSR) were performed with the number of principal components required so that the variance explained in the predicted variable (% concentration) surpassed 80%. This criteria was chosen after reviewing several Principal Components (PC) vs. Scree plots which indicated the variance explained per additional PC was diminishing beyond this point.

4.1 Raman

In this section the results of Raman measurements on pure lithium compounds, R1, and R2 are discussed. The results are organized as follows: univariate regression on R1 and R2, PCA on pure compounds, and PCR/PLSR on R1 and R1. Because the laser parameters used for pure $LiOH$ and Li_2CO_3 measurements were significantly different than those used for all other samples, these measurements were excluded from analysis of R1 and R2.

4.1.1 Univariate Regression

The univariate regressions for the Raman spectra yields RMSE and R^2 values substantially superior to those obtained by the univariate regressions performed on the LIBS data. This is not surprising considering the Raman measurement technique is a direct measure of the molecules present rather than the individual elements. The RMSE and R^2 values for R1 and R2 are (5.39, 0.926) and (3.34, 0.971) respectively. Results of these linear fits can be found in Figures 21 and 22.

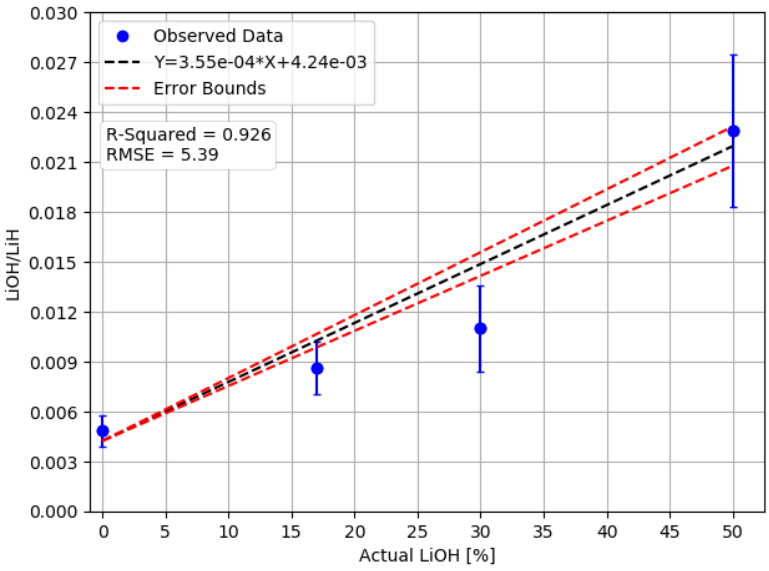

Figure 21. Univariate regression for $LiOH$ in LiH using ratio of respective molecular Raman lines.

One will notice these regressions stop at 50% concentration. Again, this is because the values for 100% were taken with different laser power settings.

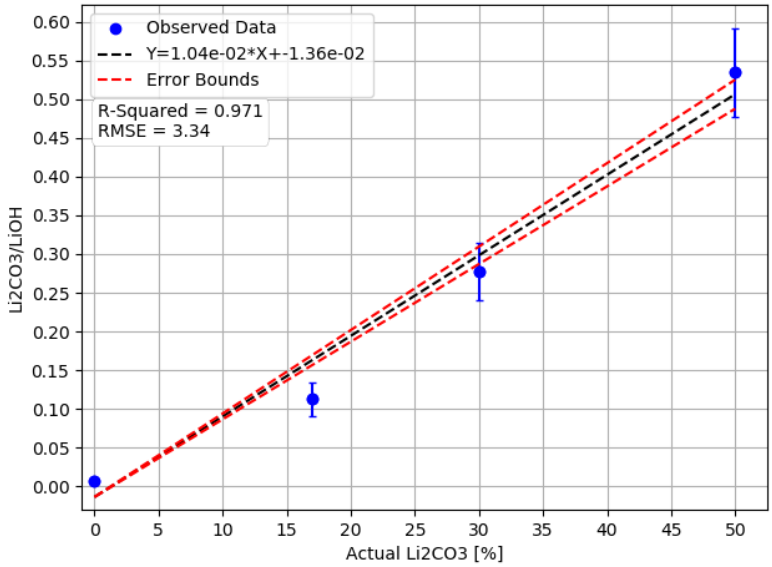

Figure 22. Univariate regression for Li_2CO_3 in $LiOH$ using ratio of respective molecular Raman lines.

4.1.2 Pure Lithium Compounds

Principal components analysis was performed on the pure samples to ensure good separation exists in principal components space and that differentiation between samples is possible using these multivariate analyses. The PC plot for Raman measurements on pure lithium compounds is shown in Figure 23.

Even at initial glance, it is evident that greater separation between samples exists for the Raman spectra than for the LIBS spectra shown in Figure 29.

4.1.3 PCR/PLSR

All but one of the analyses performed on the Raman data outperformed the same analyses performed on the LIBS data with respect to RMSE and R^2 values. The RMSE and R^2 values for R1 PCR and PLSR are (11.1, 0.736) and (10.0, 0.727) respectively. The RMSE and R^2 values for R2 PCR and PLSR are (4.30, 0.957) and

(2.29, 0.986) respectively. The results are shown in Figures 24 and 25. The one instance where Raman data did not outperform LIBS data in these analyses is the PLSR analyses conducted on R1 which yielded an RMSE value was 1.5x larger. This is surprising because the Raman measurements are directly indicative of the molecules present. One potential explanation is the relative difference in shape of the spectra from LiH versus the other two compounds. $LiOH$ and Li_2CO_3 both have very sharp Raman peaks but LiH has a very weak and broad signal more akin to a continuum (see Figures 18 and 19).

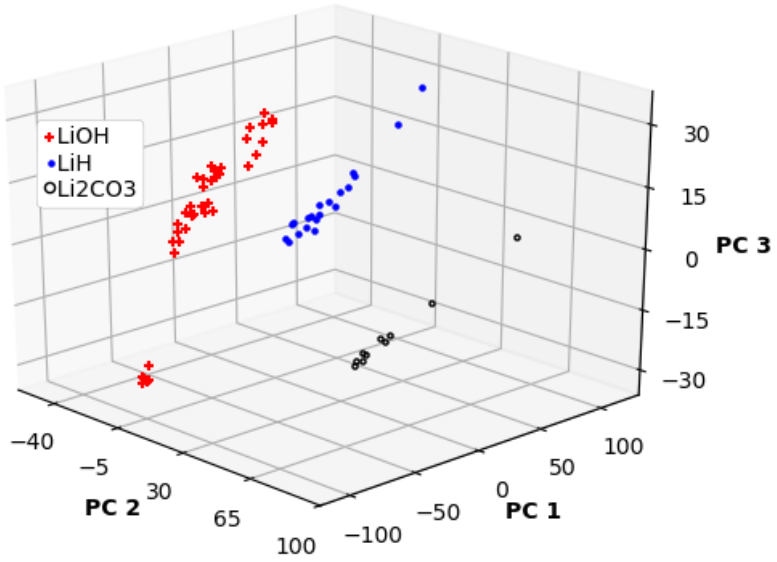

Figure 23. Demonstrating separation between Raman spectra of pure lithium compounds in principal components space.

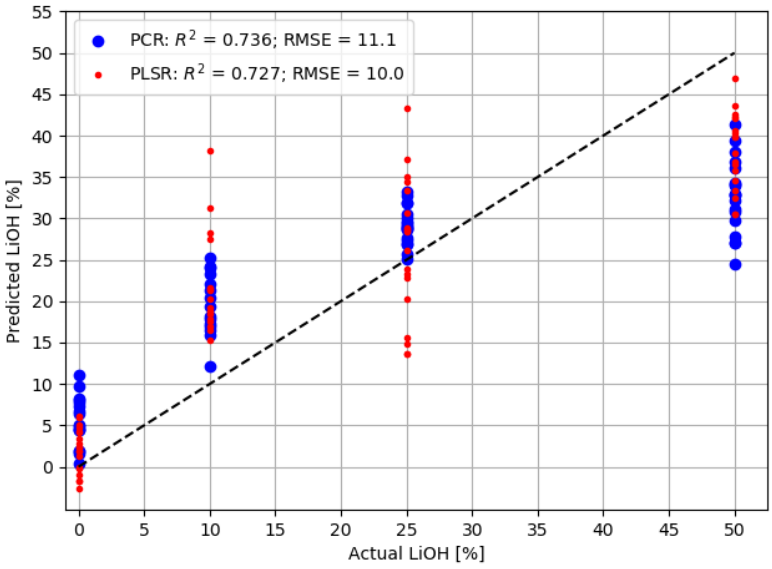

Figure 24. Comparison of Raman data using PCR and PLSR for predicting percent concentration of $LiOH$ in LiH.

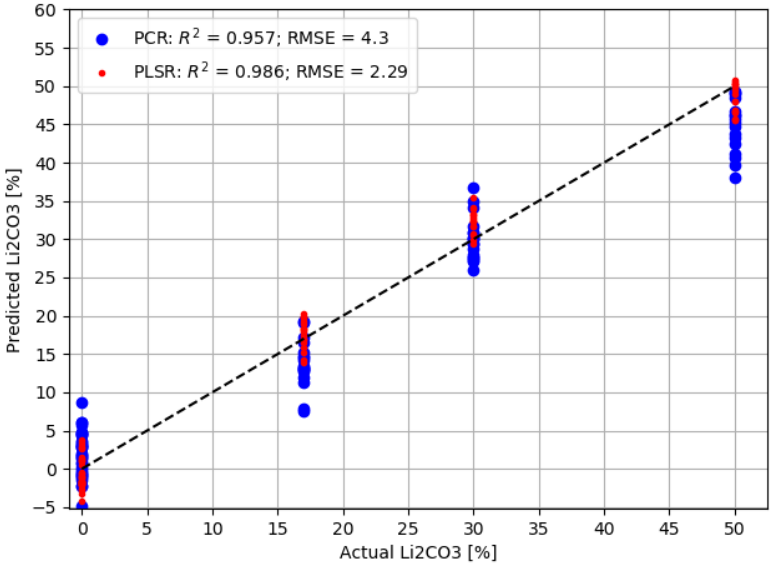

Figure 25. Comparison of Raman data using PCR and PLSR for predicting percent concentration of Li_2CO_3 in $LiOH$.

4.2 LIBS

The LIBS results are organized as follows: univariate regression on R1 and R2, PCA on pure compounds, PCR/PLSR on R1 and R1, and depth profiling.

4.2.1 Univariate Regression

The univariate regression performed on LIBS data was a linear least squares fit based on the ratio of integrated peak heights for oxygen and hydrogen. The univariate fit as a function of percent $LiOH$ is displayed in Figure 26.

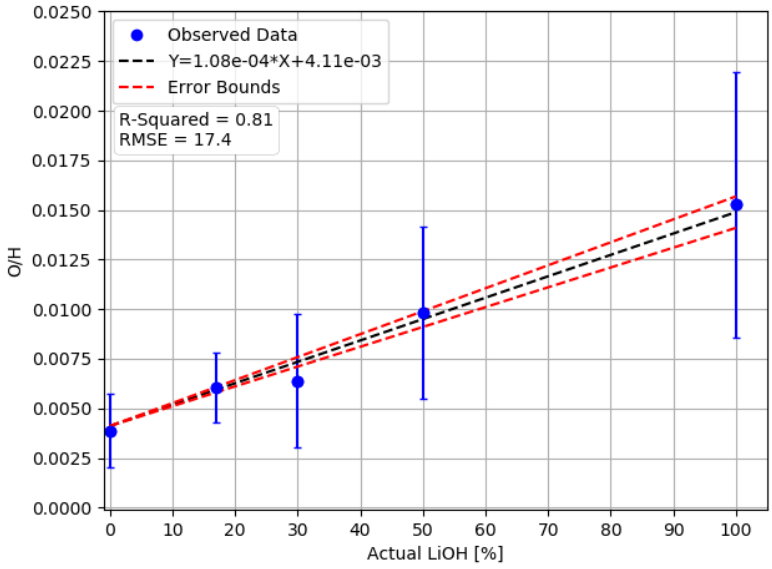

Figure 26. Univariate regression for $LiOH$ in LiH as a function of oxygen (777 nm) and hydrogen (656 nm).

The same dependent variable for R1 was also used for R2 due to failure to observe the carbon line at 833 nm on a consistent basis. The intensity of carbon lines in LIBS spectra has been observed as relatively weak by others and can be explained by the relatively high melting point of carbon and the low transition probability as compared to other elements in the sample matrix [65]. Efforts were made to enhance

the observation of this atomic emission line with little success. The carbon line at 833 nm was sometimes observed in the pure sample of Li_2CO_3 but never in a mixed sample. Therefore, it was not used in univariate regression modeling. The univariate fit of R2 with O/H is shown in Figure 27. These plots display an increased variance in

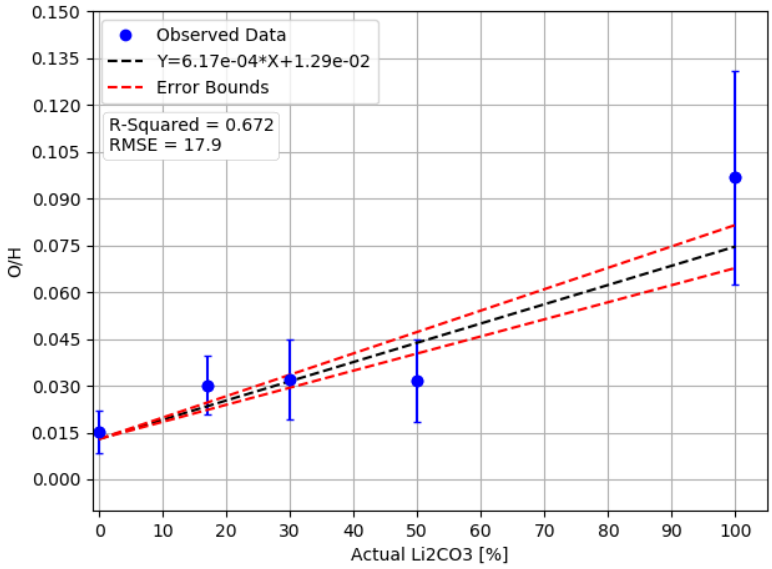

Figure 27. Univariate regression for Li_2CO_3 in $LiOH$ using ratio of oxygen (777 nm) and hydrogen (656 nm).

the ratio as O/H and percent concentration increase. This is attributed to an increase in shot-to-shot variance in the oxygen peak intensity as the oxygen concentration increased. The relative standard deviation as a function of percent concentration of $LiOH$ is shown in Figure 28.

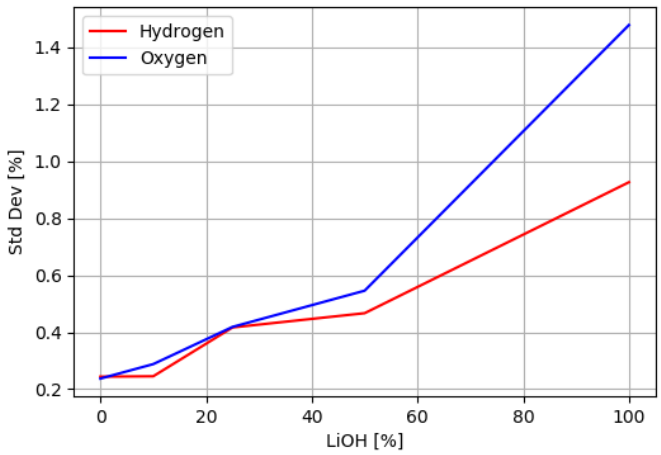

Figure 28. The relative standard deviation of the integrated line intensity for oxygen is the primary contributor to the variance in the R1 univariate regression values.

4.2.2 PCA on Pure Lithium Compounds

PCA was conducted on the samples composed of pure lithium compounds. Figure 29 demonstrates a separation does exist in principal component space for the pure samples. This makes regression modeling of these pure forms viable.

4.2.3 PCR/PLSR

Multivariate regression for the LIBS spectra was performed using the entire spectra from 550 nm to 850 nm. The intention with using the entire spectra is to allow the method to find/use underlying features which are not apparent upon cursory review of the spectra. Consideration of specific features such as single or multiple emission lines is already covered under univariate analysis. For the remaining analyses, only regression values up to 50% concentration were included. This is because Raman spectra for the 100% mixes in R1 and R2 were collected using a different laser power and were not included in analysis. In order to make a proper comparison of LIBS and Raman, the LIBS measurements for these same samples were also removed. A further

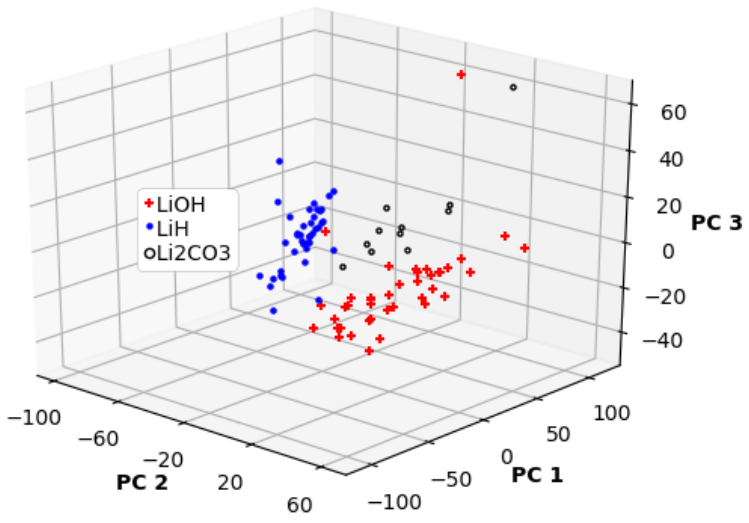

Figure 29. Demonstrating separation between LIBS spectra of pure lithium compounds in principal components space.

explanation for this was covered in Section 4.1. The (RMSE, R^2) for R1 PCR and PLSR are (11.1, 0.658) and (6.66, 0.889) respectively. The (RMSE, R^2) for R2 PCR and PLSR are (11.1, 0.685) and (3.33, 0.974) respectively. PLSR outperforms PCR in both regressions and regressions for R2 were more accurate than for R1 as shown in Figures 30 and 31. This is because PLSR uses both the dependent and independent variables to build the model while PCR only uses the independent variables.

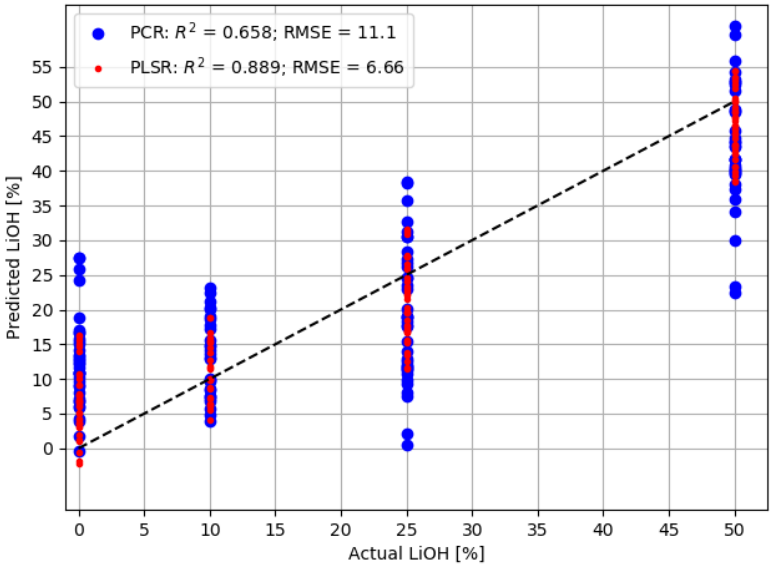

Figure 30. Comparison of LIBS data using PCR and PLSR for predicting percent concentration of $LiOH$ in LiH.

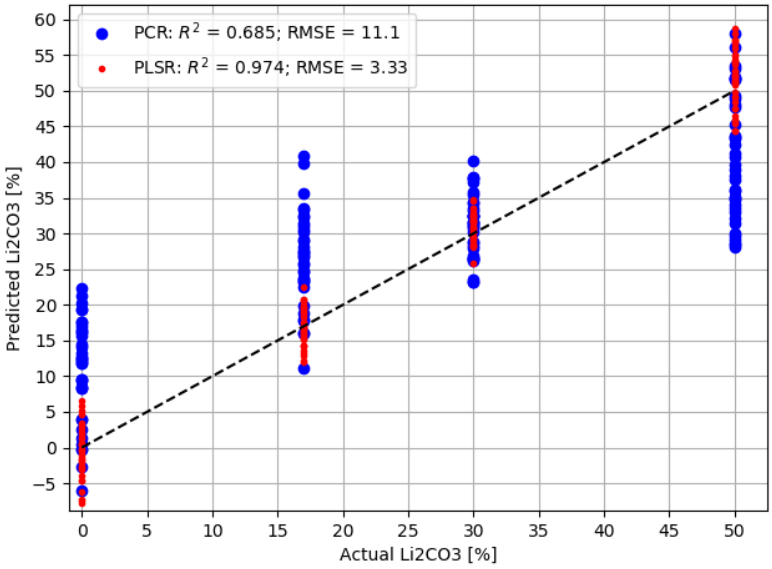

Figure 31. Comparison of LIBS data using PCR and PLSR for predicting percent concentration of Li_2CO_3 in $LiOH$.

4.2.4 Depth Profiling

Due to the removal of material from each ablation, LIBS lends itself to depth profiling where a layer by layer analysis of the elements in the sample is conducted. While the cratering rate (depth per ablation) is consistent in the samples studied, there are a couple of aspects which degrade the efficacy of this technique. The aspects of concern are the chemical composition of the sample local to the crater and preferential ionization.

First, in order to properly quantify this layer by layer analysis, the cratering rate was quantified. The results of crater measurements are presented below in Table 6. In total, 10 craters were measured each created with 20 ablations.

Concern arose when the oxygen peak in one spectra was observed clearly but a subsequent spectra taken from the same position showed nearly no oxygen (see Figure 32). There are at least two potential causes for this loss: change in chemical composition and/or preferential ionization.

Table 6. Results of depth measurements from 10 ablation craters after 20 ablations in each crater.

	Avg Depth (μm)	Std. Dev. (μm)
Crater	211.9	39.9
Per Ablation	10.6	1.5

LIBS was conducted using a nanosecond pulse laser; as such the primary excitation mechanism for plasma production is thermal. It has been observed that nanosecond pulsed lasers have a thermal diffusion length of approximately 1 μm in metals [45]. This diffusion length determines how deep melting, layer mixing, and preferential volatilization occurs in the sample. With ablation depths of 10 μm per pulse, these thermal effects are expected to have an impact on subsequent ablations in the same position on the sample. Another potential cause of change to chemical composition is preferential volatilization. This occurs when certain elements become volatile more

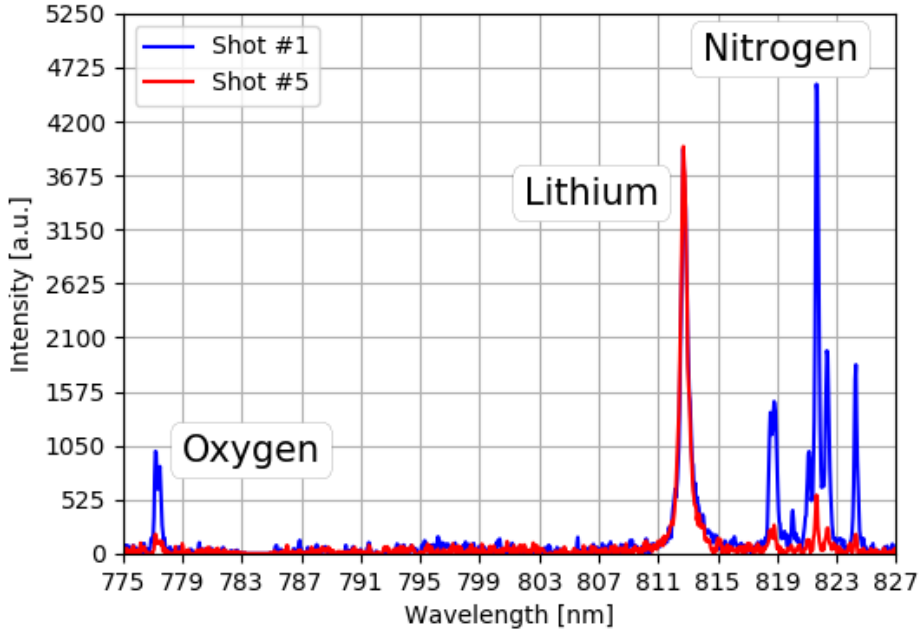

Figure 32. A comparison of two LIBS spectra from the same sample just a few shots apart shows dramatic changes attributable to matrix effects in the sample.

easily than others and thus remove themselves physically from the sample matrix. The behavior of the spectra in Figure 32 is characteristic of preferential volatilization.

The other concern is that of preferential ionization. This occurs when elements of lower ionization energy preferentially absorb the laser energy leaving less for the other constituents [28,48]. Evidence to support this is found in the peak intensities of hydrogen, oxygen, nitrogen and lithium. Hydrogen, oxygen and nitrogen have similar ionization energies of 13.6 eV, 13.6 eV and 15.6 eV respectively. Lithium has an ionization energy of 5.4 eV. The hydrogen, oxygen and nitrogen peaks vary greatly from shot to shot but maintain consistent proportions to one another, meanwhile the lithium peak intensity at 812 nm is consistent and thus does not maintain a proportion to either nitrogen or oxygen peaks.

These same effects were not observed on the first shot of each position within the same sample. That is, the spectra of the first shot in each position have consistent

peak intensities. This means the change in the spectra following the first shot in each position is explainable by some change in the sample caused by the ablation process.

The inconsistent spectra as a function of depth raise concern for using this data in depth profiling. This study does not pursue depth profiling beyond this point. However, modifications can be made to the experiment which will make depth profiling viable. Suggestions for these modifications can be found in Section 5.1. Similar inconsistencies in spectra as a function of depth were observed by Basler et al. when using a nanosecond pulse laser in depth profiling coatings on copper metals [66].

However, others have succeeded in performing depth profiling with nanosecond, and even microsecond, LIBS [67–69]. What sets this study of lithium compounds apart from these other studies is two-fold. One, the elements of interest in these other studies have ionization energies much lower than those for oxygen and nitrogen. For example, some of the primary elements of interest include iron (7.9 eV), titanium (6.8 eV), potassium (4.3 eV), sodium (5.1 eV), and magnesium (7.6 eV). The ionization energies (listed in parentheses) of these elements are approximately half that of oxygen (13.6 eV). Because of this, they are less likely to suffer from preferential ionization. The second aspect that sets this study apart from others is the spectral bandwidth of the setup. The most intense atomic emission from carbon is at 165.7 nm which is well below the cutoff of 550 nm in this setup. The only observable carbon line (833 nm) has an intensity three orders of magnitude lower. Even when optimized, this setup was unable to observe this carbon line with consistency.

A final consideration when assessing the reason why nanosecond pulsed LIBS was unsuccessful in this study when compared to others is the physical matrix effects. Two of the three studies cited above were conducted on metals [67, 69] and the third was conducted on commercially acquired tablets coated with titanium [68]. Those samples were far less likely to experience pulverization which would lead to a lower density

of material in subsequent ablations. The pellets in this study were far more likely to experience physical matrix effects due to their untreated, un-coated, pressed powder form. Consequently, it is hypothesized the sample material was made less dense by pulverization or settling of material ejected from the sample surface. The lower density led to lower plasma temperature in subsequent ablations which consequently exaggerated the effects of preferential ionization.

4.3 Data Fusion: A Pseudo-Spectra

Only multivariate analyses were performed on the pseudo-spectra created through data fusion. The expectation is the analysis will yield higher R^2 values and lower RMSE values.

4.3.1 PCR/PLSR

PCR and PLSR were performed on both R1 and R2 fused data sets. Interestingly, the results indicate a lack of improvement in a couple of cases. First is the lack of improvement for the PCR results on R1 (RMSE, R^2 = 10.2, 0.735), these can be seen in Figure 33. But the PLSR performed on R1 outperforms (RMSE, R^2 = 2.46, 0.984) any regression on R1 in this study with an RMSE less than half of that of the next best regression (Raman, feature selection)(see Table 7). The results of PCR and PLSR for R2 fusion data are superior to those from LIBS but inferior to those from Raman data. The RMSE and R^2 values for R2 PCR and PLSR are (6.67, 0.874) and (2.47, 0.982) respectively. These results are displayed in Figure 34. A full set of quantified results is in Table 7. The decline in performance going from Raman data to fusion data for R2 is inherently due to the introduction of the LIBS data. The improvement in performance for R1 using PLSR while a decline in performance for R2 is observed is unexpected, especially considering the PLSR results for LIBS data

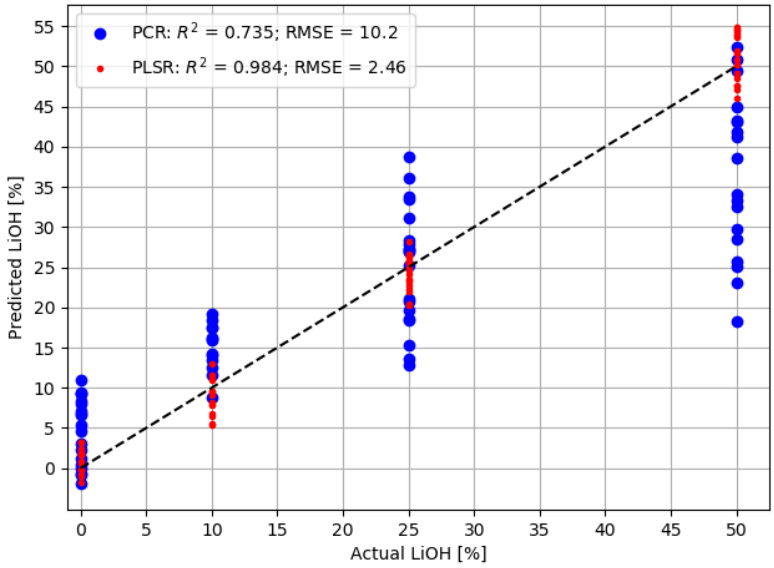

Figure 33. Comparison of fusion data using PCR and PLSR for predicting percent concentration of $LiOH$ in LiH.

from R2 outperformed those from R1. The reason for these disparate responses is unknown.

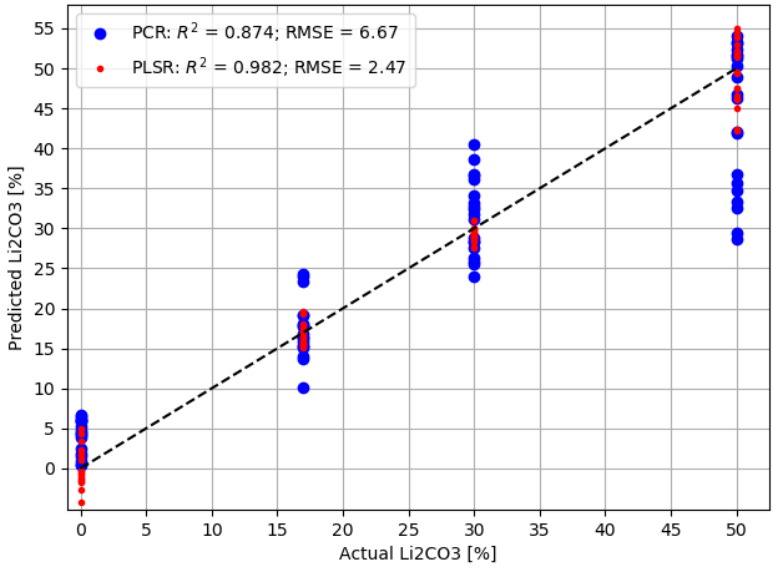

Figure 34. Comparison of fusion data using PCR and PLSR for predicting percent concentration of Li_2CO_3 in $LiOH$.

4.4 Trends

This section is dedicated to drawing attention to trends observed in the data and analyses. Table 7 lists the performance metrics of each analysis performed. These values are the basis for the discussion that follows.

Table 7. Performance metrics across all measurement and analysis combinations.

Regression	Measurement	Analysis	R^2	RMSE
R1	LIBS	Feat.Sel.	0.665	13.5
		PCR	0.658	11.1
		PLSR	0.889	6.66
	Raman	Feat.Sel.	0.926	5.39
		PCR	0.736	11.1
		PLSR	0.727	10.0
	Fusion	PCR	0.735	10.2
		PLSR	0.984	2.46
R2	LIBS	Feat.Sel.	0.432	21.4
		PCR	0.685	11.1
		PLSR	0.974	3.33
	Raman	Feat.Sel.	0.971	3.34
		PCR	0.957	4.30
		PLSR	0.986	2.29
	Fusion	PCR	0.874	6.67
		PLSR	0.982	2.47

First, the performance of regressions performed on R2 always outperform those performed on R1 (all else constant) with exception of fusion data using PLSR. This can be traced back to the elemental composition and difference in number density of the compounds. In R1, the difference between the two compounds in the mixtures is a single oxygen atom per molecule. In R2, the difference between the two compounds is three fold: (1) a single hydrogen atom, (2) a single carbon atom, and (3) two oxygen atoms. As previously discussed, the carbon emission is of little consequence. However, the hydrogen emission line is a prominent feature. The oxygen peak at 777 nm is not as strong as the hydrogen peak on a per-atom basis but it is observable

even in pure $LiOH$, thus there is a sufficient difference in the spectra when tripling the number density of oxygen as such is the case in R2.

Secondly, PLSR always outperforms PCR within the same data set. PLSR is very similar to PCR. They both find latent variables within the explanatory variables of the data (in spectra, these are the wavelengths, or more fundamentally the channels on the spectrograph). They both seek to maximize the variance in the data explained by the principal components. The difference is PLSR uses both the explanatory and dependant variables. PLSR seeks to minimize the covariance between the explanatory and dependant variables. Thus, it is not surprising PLSR outperforms PCR in these data sets.

4.5 A Concerning Observation

An unexpected concern with conducting LIBS measurements for the purpose of characterizing lithium compounds associated with lithium hydride arose while ablating pellets containing LiH. The samples charred black in the area surrounding the ablation crater. Initially the concern was the lithium hydride was reacting with nitrogen to form any of three compounds (Li_3NH_4, Li_3NH_2, Li_2NH). These compounds have been known to form when lithium hydride is heated in the presence of nitrogen to 160^{o}C, 340^{o}C, and 600^{o}C respectively [18]. Upon further observation, however, the black marks on the hydride pellets reduced over the course of several days merely sitting in the cell. This led to further investigation. Raman spectra were taken in order to observe whether the black marks were composed of compounds indicative of the previously mentioned compounds. However, the spectra revealed zero spectral features. After conducting Raman measurements on the burnt samples, it was observed the black marks were nearly completely gone and the sample returned to it's original appearance with exception of the area in the immediate vicinity of the

craters. This may be a result of lithium hydride being subject to photochromism. As noted in the lithium hydride safety card, it is subject to darkening upon exposure to light [30]. Figure 35 displays the color change of lithium hydride which occurred as a result of ablation and Raman on the black marks which followed ablation. Samples

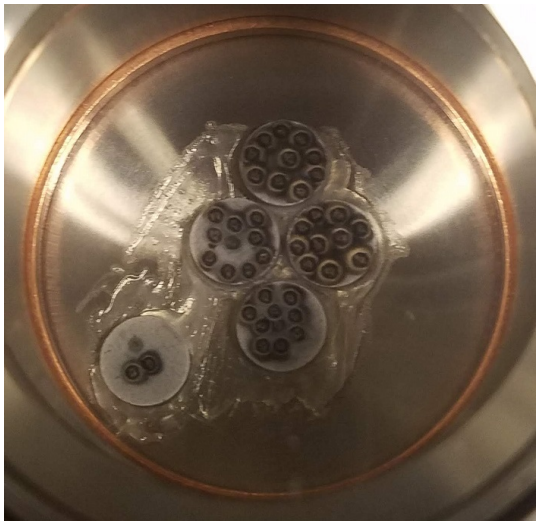

Figure 35. Dark charring marks on pure LiH samples indicative of thermal reactions, photochromism or both.

1 and 2 have been ablated but not measured via Raman spectroscopy. Sample 3 has been ablated and measured via Raman in position 4 for one spectra (5 min at 10Hz). Sample 4 has also been ablated but was measured via Raman for two spectra (total of 10 min at 10Hz). The sample off to the side is an additional pellet produced for testing measurement parameters prior to ablating the samples used in analysis. This "test" sample provides a visual for the unperturbed surface in the areas it has not been ablated.

V. Conclusions

It was demonstrated that LIBS, Raman spectroscopy, or a data fusion of the two can be paired with univariate and multivariate techniques to predict percent concentration of lithium compounds in pressed pellets. In modeling the presence of $LiOH$ in LiH, PLSR paired with data fusion performed the best with an R^2 of 0.984 and RMSE of 2.46. In modeling the presence of Li_2CO_3 in $LiOH$, PLSR paired solely with Raman data performed the best with an R^2 of 0.986 and RMSE of 2.29. The performance metrics (R^2 and RMSE) for each of the combinations are displayed in Table 7.

From Table 7 it is evident that when there is no limitation to which measurement techniques are employed, both should be used and a data fusion approach should be employed along with PLSR chemometrics. This is evident from the substantial improvement seen in R1 when compared to LIBS or Raman alone. While model performance does not improve for R2, the loss of performance is relatively small (8% increase in RMSE). Additionally, if data fusion methods are employed, the data to perform any of the individual analysis techniques is available for use.

However, there are instances where equipment, time, or both are limited. Raman spectroscopy is superior to LIBS when several minutes per sample are available and only surface data is desired. LIBS spectroscopy is superior when minutes are not available or if depth profiling is desired. While the nanosecond pulsed laser in this study was found to be insufficient for depth profiling, it has been shown pico- and femtosecond lasers have much higher depth profiling efficacy [45, 66].

This work demonstrated the capability of both LIBS and Raman to quantitatively characterize three lithium compounds (LiH, $LiOH$, and Li_2CO_3) when paired with multivariate and even univariate analysis techniques. A novel setup for conducting both LIBS and Raman using the same equipment is demonstrated with great success

utilizing a single pulsed Nd:YAG laser, assorted optics, and an echelle spectrograph. The broad bandwidth of the echelle spectrograph enabled the measurement of light from 550 nm to 850 nm, though wavelengths as low as 350 nm were possible without the light rejection optics in place for Raman measurements. This unique setup allowed for efficient use of time and lab space which is a significant advantage in labs where space and access are limited. The dual setup also minimizes potential user error when ensuring data is collected from the same sample/position for data fusion. Lastly, where commercial LIBS and Raman systems may be housed in separate facilities, this single setup minimizes potential safety concerns when transporting hazardous materials for analysis. Extension of these methods can be made to quantifying lithium compounds in samples exposed to environmental conditions.

5.1 Recommendations for Future Work

What follows are recommendations for improving the methods used in this research. These recommendations include choosing a different buffer gas, using a faster laser, and exploring employment of a bifurcated fiber.

First, this study used nitrogen as a purge gas. This was done following direct communication with a manufacturer of LiH (Sigma Aldrich) which stated the standard is to handle and store the compound under dry nitrogen atmosphere. However, LiH reacts with nitrogen at temperatures above 200^{o}C to form various other compounds [18]. This may explain the char marks displayed on the sample in Figure 35. These dark marks may also be due to photochromism which LiH has been noted to be subject to. The intense light of the plasma may have been cause for this photochromism. Under another buffer gas, such as argon or helium, any nitrogen compounds which may have been forming under nitrogen will no longer be an issue. Additionally, the use of helium as a cover gas has been shown to enhance LIBS signal [11, 41]. Using helium

or argon also allows for confirmation that constituents of the air are not present in the chamber. This is completed by viewing the nitrogen peaks, if there are no nitrogen peaks then the chamber is free of other constituents of the air which might interfere with the desired signal such as oxygen emissions [11]. Research grade helium does not need to be used for the entire sample preparation. The recommendation is to use dry nitrogen in the form of liquid nitrogen (LN) boil-off for the sample preparation since LN is cheaper and the expansion ratio from liquid to gaseous phases allows for efficient use of space and time. When the sample has been prepared, place it in an air tight cell with a gas inlet/outlet on the side which has a shutoff valve where the helium gas can be flowed into the sample cell and displace the nitrogen all the while never exposing the sample to laboratory air.

The use of a faster pulsed laser would allow for greater efficacy of depth profiling. Pico- and femtosecond pulsed laser ablation is accomplished primarily by non-thermal energy transfer [41]. Consequently, the thermal diffusion length of these laser produced plasmas is an order of magnitude smaller than that of nanosecond pulsed laser ablation [45].

The use of a bifurcated fiber will allow light from the same path to be sent to two separate measurement devices. The inherent disadvantage to this is the intensity of the light reaching the camera is cut in half at a minimum (assuming no losses at the fiber splice). The advantage is the ability to view spectral lines which maybe out of view of one instrument. While the echelle spectrograph has a very wide static field of view, there are monochrometers with a wider dynamic field of view. This would be useful if an element of interest, such as carbon, has higher intensity peaks outside the static field of view of the echelle while all other elements of interest fall within the echelle field of view.

Appendix A. Study on Pellet Pressing Parameters for analysis of $LiOH(H_2O)$ via LIBS

Optimization of Pellet Pressing Parameters for Use in Laser Induced Breakdown Spectroscopy

James Stofel, *Student, AFIT*

***Abstract*—This work explores the impacts of parameters associated with pressing pellets from LiOH (monohydrate) powder for the purpose of analysis by LIBS. Parameters investigated include pressure used to press the pellets, the presence of binder material, and whether or not the sample is ground up prior to pellet pressing. The findings indicate the optimum parameters particular to this situation are to grind the sample, not use binder, and to press the pellets with 1.5 tons of pressure.**

I. Introduction

LASER induced breakdown spectroscopy (LIBS) is a semi-nondestructive elemental analysis technique which allows for rapid analysis of gaseous, liquid, and solid samples with little or no preparation. Analysis can be conducted with the laser in close proximity to the sample or at a large stand-off. The flexibility of the technique makes it an attractive option for qualitative and quantitative elemental analysis of samples.

LIBS uses a pulsed laser to ablate the sample. Ablation occurs because the laser pulse is concentrated both in time and space. The concentration in time leads to increased power as the energy of the laser output is all delivered in a short time. The concentration in space (using a lens to focus the laser pulse) leads to increased irradiance (power per unit area). The energy from this laser pulse is deposited into the sample. The large energy density causes ionization of the atoms and an electron avalanche follows resulting in a plasma which emits light.

The light emitted from this plasma is characteristic of the elements present in said plasma. When viewed with a spectrometer, spectral lines associated with elements present in the sample are observed. This lends itself to qualitative and quantitative measurements of the sample's elemental composition. In order to take repeatable measurements with minimal variance amongst those measurements, the laser ablation process must differ as little as possible from shot to shot. The physical properties of the sample have a large impact on these shot-to-shot variations. These properties are driven by the process used to produce the samples. Optimal procedures for this production is what will be determined in this study.

Work has been accomplished in pellet pressing parameter optimization by others in the past [1]. The typical parameters of interest include coarseness of the sample prior to pressing, the use of a binding agent, and the pressure at which the pellets are pressed. Therefore, these are the same parameters which are investigated in this work as well. Though best practices are stated in the literature for pressing powder samples into pellets for analysis by LIBS, there is variation between samples based in the physical properties of the powders which lead to differing optimal parameters. For this reason, it is necessary to accomplish a parameter optimization for each sample type using the results of previous studies as a starting point [1].

According to Singh and Thakur, the optimal parameters for pressing powder pellets of californium include, grinding the powder, mixing 5% polyvinyl alcohol (PVA) into the sample, and pressing at 3,000 lbs/sq-in [1]. The process for mixing PVA into a powder sample involves creating a slurry of PVA, sample, and distilled water, then baking out the water. This alone is a prohibitive procedure for the samples of interest in this work because the procedure being optimized will be used in producing samples for studying hydrolysis reactions of lithium compounds in air. Thus, intentionally adding water to the sample is out of the question and an alternative binding material was chosen (Cereox).

II. Problem Description

Current work is being performed on powders of lithium compounds using LIBS. Results from analysis of these powders benefits greatly from pressing the powder into a pellet prior to analysis (as with almost all powders analyzed by LIBS). This is due to the nature of the technique which ablates the sample in order to analyze it. This ablation process creates a shock wave which causes ejection of material. When in loose powder form, the laser induced plasma (LIP) will eject and loft a large amount of material from the sample and thus change the surface topography of the sample. This leads to large variations in the shot-to-shot configuration of the sample and thus the LIP created at the sample. This also reduces the repeatability of the analysis technique.

The goal is to have a sample which lends itself to repeatable measurements with minimal variations between these measurements. These measurements can be from shot-to-shot or from one sample to another. Either way, the goal is to have a pellet pressing procedure which produces consistent pellets which lead to strong, uniform intensity in the spectra.

The parameters under consideration are whether or not to grind the sample, whether or not to use a binding agent, and what pressure to use in pressing the pellets. The grinding

J. Stofel was with the Department of Engineering Physics, Air Force Institute of Technology, Wright-Patterson Air Force Base, OH, 45324 USA e-mail: james.stofel@afit.edu.

parameter is binary in this experiment: either the sample is ground up or it is not ground up. The use of binding agent is also binary: either 0% or 20% binder by weight. The use of 20% is chosen as this is the recommended optimal binder percentage for pressing pellets provided by Fluxana [2]. This parameter could be further investigated to include other concentrations but the limitations of time reduced the number of concentrations to two. The press used in pelletizing the samples has a range of pressures from zero to two tons. The pressures under investigation are 1.0, 1.5, and 2.0 tons. The gauge on the press is continuous with indicators every tenth of a ton. This press is used here because it is the press which will be used in later research involving the production of these pellets. The glove-box constrains the size of the press available for use and thus the higher pressures typically used in other studies are not available in this work. These parameters together create a variety of pellet pressing options to include twelve configurations. At three samples per configuration, the test matrix includes 36 samples as shown in Table I where NGNB is "Not Ground No Binder," NGB is "Not Ground Binder," GNB is "Ground No Binder," and GB is "Ground Binder." What this work aims to accomplish is determine which of these configurations produces the best pellets.

	NGNB	NGB	GNB	GB	Total
1 ton	3	3	3	3	12
1.5 tons	3	3	3	3	12
2 tons	3	3	3	3	12
Total	9	9	9	9	36

TABLE I
NUMBER OF SAMPLES PRODUCED AND ANALYZED FOR THE GIVEN PARAMETERS.

By testing each of these sample parameters across three samples, the repeatability of the pellet pressing process will be examined and so will the repeatability of the observed measurement.

III. Description of Work

A. Pellet Pressing

The experiment begins with creating the pellets. The sample used in this analysis is LiOH (monohydrate) from Sigma Aldrich with 99.987% purity (Lot ID: 098F3751). This was chosen for its availability and because it is representative of samples to be studied in later works (contains lithium in powder form). The binder used is Cereox, which is a licowax powder produced by Fluxana [2]. The equipment needed for pellet production also included a mortar and pestle for grinding, digital lab scale, shaker, and pellet press assembly (press and dyes). Of note, the shaker was the Fluxana MUK Mixer and the pellet press assembly was the Specac Mini Pellet Press. With exception of the mortar and pestle, the pellet pressing equipment is displayed in Figure 1.

The order of operation was to measure the mass of the sample to be used in the particular batch. Remember there are nine samples to be made per sample mixture (three at each pressure). Based on initial measurements from practice pellets, approximately one gram of sample was used in each batch. This sample was then placed in the mortar and the

Fig. 1. Equipment used to press the pellets.

pestle was used to grind the sample from a coarse consistency down to a fine consistency to the point where little or no resistance was felt in the grinding motion. The ground sample was then placed in the shaker container and approximately 25 mg of Cereox was added to the sample. The exact amount of Cereox varied depending on how much LiOH powder was in the sample. The mass of Cereox was adjust to achieve 20% binder by weight. A shaker ball was then added to the container and it was then mounted in the MUK Mixer and shaken for 60 sec at level nine on the settings dial.

After mixing, the press dye was filled with the sample. The dye assembly was then placed in the press and the press was tightened down until the appropriate pressure was displayed on the gauge. The press required consistent tightening as the sample compressed under the pressure. This pressure was applied for three minutes in order to allow the pressure to fully compress the pellet uniformly. Three minutes under pressure was determined as adequate due to the gauge holding steady after this amount of time which indicated the pellet was not compressing further. The end-product pellet is displayed in Figure 2.

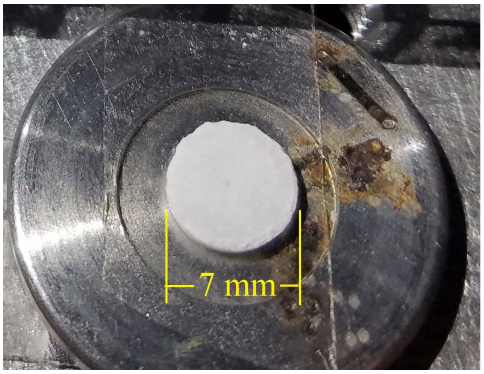

Fig. 2. One of the pellets produced in this experiment. This one was from the batch "Not Ground No Binder" pressed at 1.5 tons.

The process described thus far includes steps for producing the "Ground with Binder" sample composition. In order to create any of the other sample compositions, one only needs

to remove the aspect from the above description which would then supply the desired sample. All other steps and their order will remain the same. The final mass of the pellets

B. LIBS

As discussed above, the analysis technique used on these samples is LIBS. As such, the required equipment includes a pulsed laser, a spectrometer, assorted mirrors and assorted lenses. In addition, Schlieren imaging was included in the experiment. This provided another method for visualizing the behavior of the pellets following the ablation. Often, if the spectra from a particular shot was abnormal, the Schlieren imaging was able to provide key information for discerning why the spectra was different (position, movement, etc.).

The laser was a Quantel EverGreen2 operating at 532 nm. The power output was controlled by setting the Q-switch timing. However, the laser power experienced by the experiment was controlled using a polarizer and beam splitter as shown in Figure 3. The power on the sample side of the beam splitter was measured at 85 mJ per pulse. The laser was focused onto the sample using a 200 mm focal length lens. The light from the plasma was collimated and then focused into the spectrometer with another set of lenses. A 532 nm notch filter was placed in front of the spectrometer entrance slit to protect the ICCD camera on the spectrometer from being oversaturated.

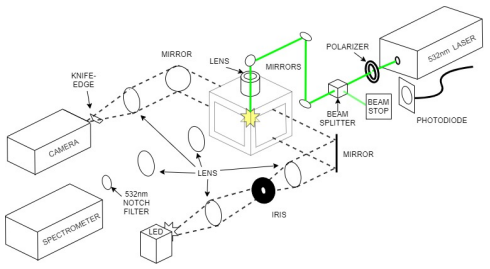

Fig. 3. Lab setup for LIBS and Schlieren.

The spectrometer used for this experiment was a Princeton Instruments HRS 750. The entrance slit to the spectrometer was set to 300 microns as determined by optimizing the signal-to-noise ratio. The gratings were set to 1200 g/mm with a blaze angle of 500 nm. The gain was set to one since the spectral line of interest was sufficiently intense as to provide max intensity greater than 10 times the background noise on average. The gate delay and width were set to 1.0 and 0.8 μsec respectively. These times were chosen in order to capture the spectra while the plasma was in local thermodynamic equilibrium (LTE). The LTE assumption is not particularly important to this experiment but later work will be conducted where LTE may be required and thus this experiment was conducted in such a manner as to mimic those conditions as much as possible.

The Schlieren imaging equipment included an LED courtesy of University of Tennessee Space Institute, a Vision Research v12.1 High Speed Camera, assorted mirrors, assorted lenses, an iris, and a razor blade. The LED flashed at a rate of 40 kHz while the high speed camera took images at the same rate in sync with the LED. This setup is also illustrated in Figure 3. Though not pivotal to this research, this imaging was instrumental in diagnosing abnormalities observed in the spectra which often manifested themselves with significantly lower intensities. For further information on Schlieren imaging, please reference the resource below from the National Aeronautics and Space Administration [3].

Due to the precision in timing required for these measurements and the diverse equipment in use (laser, spectrometer, LED, HS camera) a delay generator was used to sync them all together. The particular delay generator used here was the Berkeley Nucleonics Model 577. After arming the spectrometer and high speed camera, the delay generator enabled the user to conduct precise and repeatable measurements. The specific delay generator settings used in this experiment can be obtained from the attached digital lab notebook.

The spectral line for lithium at 610 nm was observed in this experiment. This spectral line was chosen due to it's strong intensity (second most intense of the lithium lines), it's lack of self-absorption (which is dominant in the most intense lithium line), and lack of interfering lines from other elements present in the plasma. The quality of the data was assessed to be the intensity of the spectra as well as the consistency of the intensity of the spectra both from one shot to the next as well as one sample to the next within the same sample settings. The intent was to ablate each pellet 100 times, capturing the spectra and Schlieren imaging on the first shot and every tenth shot up to 100. Due to time constraints, all 3600 shots were not collected by the spectrometer and high speed camera. One example spectra is shown below in Figure 4. Each spectra followed this approximate line shape but with varying intensities as will be discussed later in this paper.

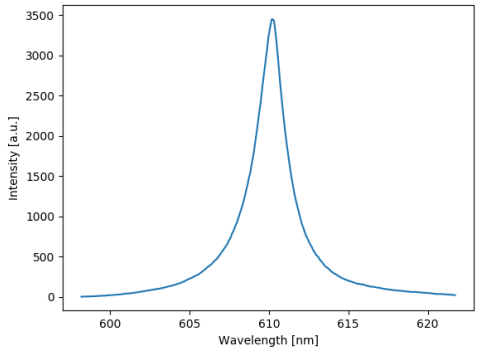

Fig. 4. Lithium spectral line at 610 nm used for comparison of pellet performance.

As mentioned before, the plasma is assumed to be in LTE during the time this spectra is captured. This is indicated by the fact the line-shape is dominated by Lorentzian broadening and Gaussian broadening is minimized. When setting the spectrometer gate delay and width, this effect can be visualized by observing the change in line-shape as the parameters are varied. Which broadening is dominant can be confirmed

by modeling the spectra with a Voigt profile which is a convolution of Lorentzian and Gaussian profiles. Using a code in Python, Voigt models were fit to every spectra taken in this dataset. The output of the model provides how much of the lineshape (represented by full width half maximum (FWHM)) is attributable to Lorentzian and Gaussian shapes. An example of a Voigt profile fit to one of the spectra in this experiment is displayed in Figure 5. For this particular spectral line, the results of the fit are shown in Figure 6. The parameter sigma is the FWHM attributable to Gaussian shape and gamma is the half width half max (HWHM) attributable to Lorentzian shape. As is shown here, Gaussian broadening in this spectra is negligible. This confirms the LTE assumption is valid for this spectra.

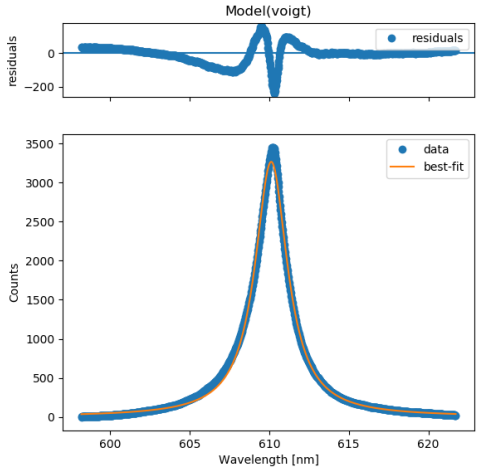

Fig. 5. This shows the spectral line can be fit with a Voigt model.

```
[[Variables]]
    amplitude:  12772.2318 +/- 39.0160412 (0.31%) (init =
17217.12)
    center:     610.130636 +/- 0.00325082 (0.00%) (init =
610.1145)
    sigma:      3.3901e-05 +/- 6.99845866 (20643678.85%)
(init = 0.7203356)
    gamma:      1.24415094 +/- 0.00460538 (0.37%) (init =
0.7)
    fwhm:       2.48830947 +/- 0.00974237 (0.39%) ==
```

Fig. 6. FWHM values from the Voigt fit.

The nature of the residuals for the model fit suggest the peak of the spectra is not captured correctly. After some deliberation and investigation, the issue remained unresolved. The asymmetry in the spectral line may be due to electromagnetic fields in the plasma which cause what is known as Stark shift [4]. The data, however, for the purpose of this experiment remains valid. This is because the area above and below the zero line in the residuals plot is approximately the same, leading to a net error in the area under the curve at or near zero. The area under the curve is what is considered for the intensity in this experiment and thus the data remains valid for this purpose.

IV. Results

Though the intent was to shoot each pellet 100 times, that did not happen for at least two sets of pellets. These were both of the "Not Ground" sets of pellets pressed at two tons. In both of these sets, the pellets shattered or sheared after no more than 50 shots. This is displayed in Figures 9, 10, and 11 in the Appendix. Comparisons were made within sample makeup and within pressure. All of the plots are included in the Appendix.

Also of note is the increase in standard deviation for the pellets pressed "Ground with Binder" at shot values higher than 60. When reviewing the Schlieren videos, these pellets were experiencing breakthrough of the laser. That is, the laser was tunneling all the way through the pellet prior to completion of the shot series. This is due to the fact that these pellets were thinner than the rest of the pellets which was a result of material squeezing out of the dye when the pellets were pressed. The cause for material escaping the dye for only these pellets us unknown but may be due to the Cereox being pushed out when pressure was applied. Though the same effect was not observed with the "Not Ground with Binder" pellets.

The most telling of the comparison plots is Figure 7 which displays the performance of all the sample makeups pressed at 1.5 tons.

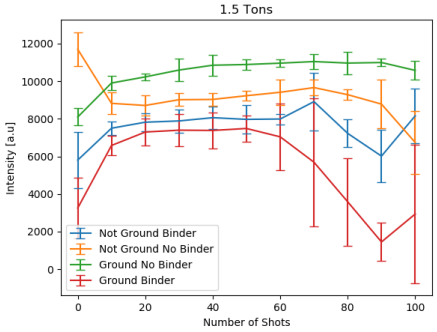

Fig. 7. Comparison of pellets pressed at 1.5 tons demonstrating "Ground No Binder" pressed at 1.5 tons produces uniform, high intensity spectra.

The remaining comparisons in the Appendix tell the rest of the story. The error bars present in the plots represents the standard deviation among the three samples in the set which matches the configuration. Further handling of uncertainty within the intensity calculations of each of the spectra was not drawn out but is available within the output of the Voigt fitting model within Python. The uncertainty associated with the amplitude for the spectra in Figure 5 is: $Amplitude = 12772 \pm 39.016\ (0.31\%)$. The units for this result are arbitrary but represent intensity. Admittedly this is the uncertainty of the model itself, not taking into consideration the residuals.

V. Conclusion

Pellet pressing for use in LIBS is not a one-size-fits-all procedure. There are good practices and starting points established and reported in the field. However, optimal parameters will

vary and may not always follow the trends one might expect. For example, this study shows that higher pressures do not provide better pellets because they end up being too brittle for repeated ablation beyond 30 or 40 shots. Additionally, binder material such as Cereox does not necessarily improve performance as it is marketed. The introduction of non-sample material dilutes the sample concentration which lowers the intensity of the spectral lines under observation. One parameter which is universally shown to improve performance is grinding the sample prior to pressing. This has been established industry wide and was further supported in this study. What came as somewhat of a surprise is the optimal pellet pressing parameters which were "Ground No Binder" pressed at 1.5 tons. Even when the comparison between pellets is limited to "valid" data, which would exclude any spectra beyond the 60 shots where "Ground with Binder" experienced tunneling breakthrough, the top result was the same: "Ground No Binder" pressed at 1.5 tons.

Further work might include a larger test matrix to include 0.5 tons for pressure and varying levels of binder to include 5%, 10%, 15%, 25% mass concentration. Additionally, the process would benefit greatly from automation which would allow the user to collect data from every single shot and not just every tenth shot.

APPENDIX

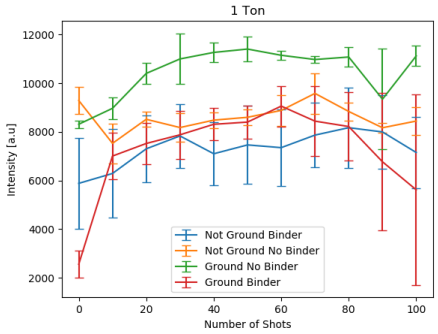

Fig. 8. Comparison of pellets pressed at 1 ton.

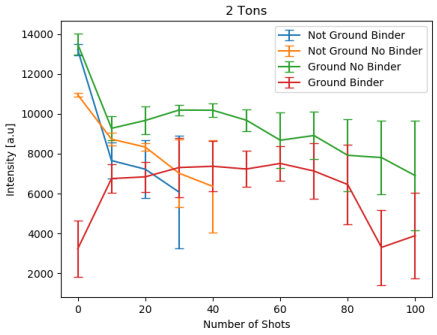

Fig. 9. Comparison of pellets pressed at 2 tons.

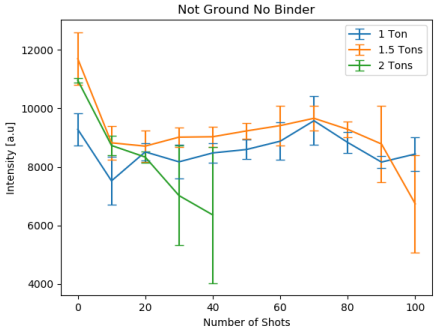

Fig. 10. Comparison of pellets prepared without grinding and without binder added.

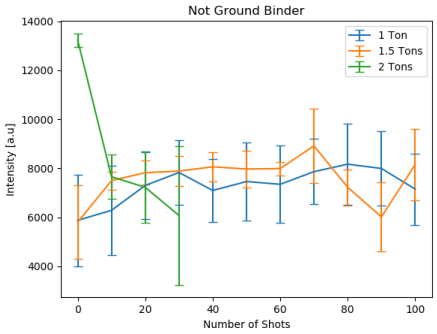

Fig. 11. Comparison of pellets prepared without grinding and with binder added.

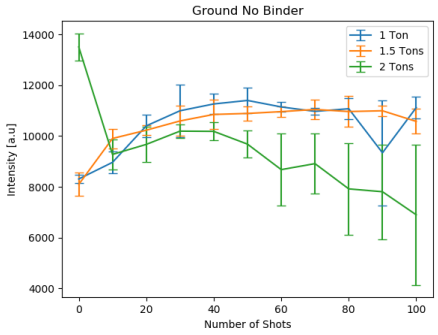

Fig. 12. Comparison of pellets prepared with grinding and no binder added.

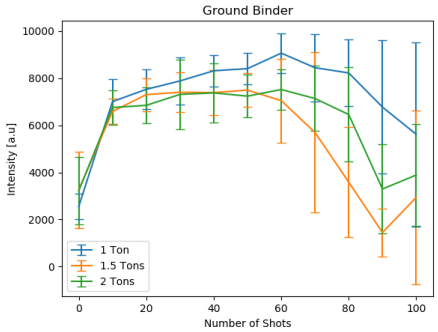

Fig. 13. Comparison of pellets prepared with grinding and binder added.

ACKNOWLEDGMENT

The author would like to thank Dr. James Bevins, Dr. Michael Shattan, Dr. Mark Gragston, and Mr. Michael Rynders for assistance in setting up this lab and helpful feedback along the way.

REFERENCES

[1] J. P. Singh and S. N Thakur, *Laser Induced Breakdown Spectroscopy*, 1st ed. Oxford, United Kingdon: Elsevier, 2007.

[2] "*Binder for Creating Pressed Pellets in XRF - FLUXANA*," Accessed on: Sep. 17, 2020. [Online]. Available: https://fluxana.com/products/pressing/binder

[3] "*Schlieren System*," Acessed on: Sep. 18, 2020. [Online]. Available: https://www.grc.nasa.gov/www/k-12/airplane/tunvschlrn.html

[4] A. M. E. Sherbini, A. E. E. Sherbini, C G. Parigger, "Measurement of Electron Density from Stark Broadened Spectral Lines Appearing in Silver Nanomaterial Plasma," *Atoms*, vol. 6, no. 44, Aug. 2018.

Bibliography

1. F. H. Welch, "Lithium hydride: A space age shielding material," *Nuclear Engineering and Design*, vol. 26, no. 3, pp. 444 – 460, 1974. [Online]. Available: http://www.sciencedirect.com/science/article/pii/002954937490082X

2. Kirk-Othmer, "Lithium and lithium compounds," in *Kirk-Othmer Encyclopedia of Chemical Technologies*, 4th edition, Hoboken, NJ, USA: Jon Wiley & Sons, 2007, p. 450. [Online].

3. G. A. Nazri *et al.*, "Lithium hydride negative electrode for rechargeable lithium batteries," United States of America Patent US7 736 805B2, June 15, 2010.

4. "Lithium Carbonate," WebMd. https://www.webmd.com/drugs/2/drug-5887-42/lithium-carbonate-oral/lithium-oral/details (accessed Jan. 30, 2021).

5. M. B. Shuai *et al.*, "Hydrolysis Characteristics of Polycrystalline Lithium Hydride Powders and Sintered Bulk," *International Journal of Materials and Metallurgical Engineering*, vol. 5, no. 11, pp. 1573–1577, 2011. [Online]. Available: https://doi.org/10.5281/zenodo.1073128

6. M. Chu *et al.*, "The solid reaction of lithium hydride and lithium hydroxide in lithium hydride pellet under normal condition and the application of CO 2 for long-time storage," *Applied Surface Science*, vol. 447, pp. 673–676, 2018. [Online]. Available: https://doi.org/10.1016/j.apsusc.2018.04.024

7. J. Guichard *et al.*, "Hydrolysis of lithium hydride under low relative humidity," *International Journal of Hydrogen Energy*, vol. 40, pp. 12 736–12 744, 2015. [Online]. Available: http://dx.doi.org/10.1016/j.ijhydene.2015.07.047

8. S. M. Matt *et al.*, "Moisture Corrosion of LiH: A Kinetic Investigation by DRIFT Spectroscopy," *Journal of Physical Chemistry A*, vol. 124, no. 2, pp. 283–287, 2020.

9. A. C. Stowe and N. Smyrl, "Raman spectroscopy of lithium hydride corrosion: Selection of appropriate excitation wavelength to minimize fluorescence," *Vibrational Spectroscopy*, vol. 60, pp. 133–136, 2012. [Online]. Available: http://dx.doi.org/10.1016/j.vibspec.2012.01.018

10. V. S. Gorelik *et al.*, "Raman spectra of lithium compounds," *Journal of Physics: Conference Series*, vol. 918, no. 1, 2017.

11. N. Ponzio, J. Woodward, and A. C. Stowe, "Investigation of Oxidation Surface Reactions on LiH Utilizing Laser Induced Breakdown Spectroscopy (LIBS)," Consolidated Nuclear Security, LLC, Y-12 National Security Complex and Pantex Plant, Oct. 2014.

12. A. Sifuentes, A. C. Stowe, and N. Smyrl, "Determination of the role of Li2O on the corrosion of lithium hydride," *Journal of Alloys and Compounds*, vol. 580, pp. S271–S273, 2013. [Online]. Available: http://dx.doi.org/10.1016/j.jallcom.2013.02.046

13. C. Maupoix *et al.*, "Experimental investigation of the grain size dependence of the hydrolysis of LiH powder," *Powder Technology*, vol. 208, pp. 318–323, 2011. [Online]. Available: http://dx.doi.org/10.1016/j.powtec.2010.08.023

14. A. Anderson and F. Luty, "Raman scattering, defect luminescence, and phonon spectra of Li7H, Li6H, and Li7D crystals," *Physical Review B*, vol. 28, no. 6, pp. 3415–3421, 1983.

15. M. H. Brooker and J. Wang, "Raman and infrared studies of lithium and cesium carbonates," *Spectrochimica Acta Part A: Molecular Spectroscopy*, vol. 48, no. 7, pp. 999–1008, 1992.

16. G. Weber *et al.*, "New insight on the lithium hydride–water vapor reaction system," *International Journal of Hydrogen Energy*, vol. 43, no. 50, pp. 22 557–22 567, 2018. [Online]. Available: https://doi.org/10.1016/j.ijhydene.2018.10.089

17. J. L. Modisette, "Investigation of Lithium Hydride and Magnesium as High-Temperature Internal Coolants with Several Skin Materials," Langley Aeronautical Laboratory, Langley Field, VA, NACA RM L58B17, May, 1958.

18. R. L. Smith and J. W. Miser, "Compilation of the Properties of Lithium Hydride," Lewis Research Center, Cleveland, OH, NASA Technical Memorandum X-483, Jan. 1963.

19. C. Haertling, R. J. Hanrahan, and R. Smith, "A literature review of reactions and kinetics of lithium hydride hydrolysis," *Journal of Nuclear Materials*, vol. 349, pp. 195–233, 2006.

20. L. N. Dinh *et al.*, "The nature and effects of the thermal stability of lithium hydroxide," *Journal of Nuclear Materials*, vol. 317, pp. 175–188, 2003.

21. J. W. Frazer and C. W. Schoenfelder, "Determination of lithium carbonate in lithium hydride," University of California Radiation Laboratory, Livermore, CA, UCRL-4918, 1957. [Online]. Available: https://babel.hathitrust.org/cgi/pt?id=mdp.39015077592841&view=1up&seq=3

22. C. E. Holcombe, "Retardation of the Reaction of Lithium Hydride with Water Vapor," Oak Ridge Y-12 Plant, Oak Ridge, TN, UC-4 Y-1835, July 1972.

23. M. Otto, "What is Chemometrics?" in *Chemometrics: Statistics and Computer Application in Analytical Chemistry*, 3rd ed. John Wiley & Sons, Ltd., 2016, ch. 1, pp. 1–13.

24. D. E. Anderson *et. al.*, "Characterization of libs emission lines for the identification of chlorides, carbonates, and sulfates in salt/basalt mixtures for the application to msl chemcam data," *Journal of Geophysical Research: Planets*, vol. 122, no. 4, pp. 744–770, 2017.

25. T. Zhang, H. Tang, and H. Li, "Chemometrics in laser - induced breakdown spectroscopy," *Journal of Chemometrics*, vol. 32, no. 11, pp. 1–18, 2018.

26. C. B. Stipe *et al.*, "Laser-induced breakdown spectroscopy of steel: A comparison of univariate and multivariate calibration methods," *Applied Spectroscopy*, vol. 64, no. 2, pp. 154–160, 2010.

27. C. R. Bhatt, F. Y. Yueh, and J. P. Singh, "Univariate and multivariate analyses of rare earth elements by laser-induced breakdown spectroscopy," *Applied Optics*, vol. 56, no. 8, p. 2280, 2017.

28. D. Cremers and L. Radziemski, *Handbook of Laser-Induced Breakdown Spectroscopy*, 2nd ed. West Sussex, UK: John Wiley & Sons, Ltd., 2013.

29. "What is Raman Spectroscopy," Horiba. https://www.horiba.com/en_en/raman-imaging-and-spectroscopy/ (accessed Jan 12, 2021).

30. *Lithium Hydride*. ICSC 0813, International Labor Organization, April 2014. [Online]. Available: https://www.ilo.org/dyn/icsc/showcard.display?p_version=2&p_card_id=0813 [Accessed: 2021-01-14]

31. B. Dutrow, "X-ray Powder Diffraction (XRD)," Geochemical Instrumentation and Analysis. https://serc.carleton.edu/research_education/geochemsheets/techniques/XRD.html (accessed Jan. 14, 2021).

32. "What is X-Ray Diffraction Analysis (XRD) and How Does It Work?" TWI, LTD. https://www.twi-global.com/technical-knowledge/faqs/x-ray-diffraction (accessed Jan. 14, 2021).

33. "Comparison of Complimentary Techniques," University of Surrey. https://www.surrey.ac.uk/sites/default/files/comparison-of-complementary-techniques.pdf (accessed Jan. 14, 2021).

34. "What is X-Ray Photoelectron Spectroscopy (XPS)?" Thermo Fisher Scientific. https://xpssimplified.com/whatisxps.php (accessed Jan 15, 2021).

35. T. Rizzuto, "Technical Note – Vibrational Spectroscopy: Infrared vs. Raman," StellarNet Inc. https://www.stellarnet.us/vibrational-spectroscopy-infrared-vs-raman/ (accessed Jan. 15, 2021).

36. "Sir Chandrasekhara Venkata Raman: Biographical," The Nobel Prize Outreach. https://www.nobelprize.org/prizes/physics/1930/raman/biographical/ (accessed Jan 15, 2021).

37. Deepak, "What are the differences between Raman and IR Spectroscopy?" Auriga Research Private Limited. https://lab-training.com/2015/06/26/what-are-the-differences-between-raman-and-ir-spectroscopy/ (accessed Jan 15, 2021).

38. "What is Raman Spectroscopy?" AZO Materials. https://www.azom.com/article.aspx?ArticleID=15797 (accessed Jan. 15, 2021).

39. S. D. George and V. B. Kartha, "A hyphenated echelle LIBS-Raman system for multi-purpose applications," *Review of Scientific Instruments*, vol. 89, no. 073108, 2018. [Online]. Available: http://dx.doi.org/10.1063/1.5024966

40. K. M. M. Shameem *et al.*, "Echelle LIBS-Raman system : A versatile tool for mineralogical and archaeological applications," *Talanta*, vol. 208, no. 120482, 2020. [Online]. Available: https://doi.org/10.1016/j.talanta.2019.120482

41. J. P. Singh and S. N. Thakur, Eds., *Laser-Induced Breakdown Spectroscopy.* Amsterdam, The Netherlands: Elsevier, 2007.

42. "Laser-Induced Breakdown Spectroscopy: Educational Notes," Teledyne Princeton Instruments. https://www.princetoninstruments.com/learn/laser-induced-breakdown-spectroscopy (accessed Jan 15, 2021).

43. D. Harvey, "Atomic Emission Spectroscopy," LibreTexts. https://chem.libretexts.org/Under_Construction/Purgatory/Book%3A_Analytical_Chemistry_2.0_(Harvey)/10_Spectroscopic_Methods/10.7%3A_Atomic_Emission_Spectroscopy (accessed Jan. 15, 2021).

44. Chegg. https://d2vlcm61l7u1fs.cloudfront.net/media(accessed Feb. 9, 2021).

45. M. D. Luque de Castro and J. L. Luque Garcia, "Acceleration and Automation of Solid Sample Treatment," *Techniques and Instrumentation in Analytical Chemistry*, vol. 24, pp. 435–499, 2002.

46. H. A. Ardakani and S. H. Tavassoli, "Depth profile analysis of nanometric layers by laser-induced breakdown spectroscopy," *Journal of Applied Spectroscopy*, vol. 80, pp. 153–157, 2013. [Online]. Available: https://link.springer.com/article/10.1007%2Fs10812-013-9738-z [Accessed: 2021,01,30]

47. L. M. Cabalín *et al.*, "Deep ablation and depth profiling by laser-induced breakdown spectroscopy (LIBS) employing multi-pulse laser excitation: Application to galvanized steel," *Applied Spectroscopy*, vol. 65, no. 7, pp. 797–805, 2011. [Online]. Available: https://doi.org/10.1366/11-06242

48. J. Wood, "Determination of lithium isotope concentration by laser induced breakdown spectroscopy using chemometrics," M.S. thesis, Dept. Eng. Phys., Air Force Institute of Technology, Wright-Patterson AFB, OH, USA, 2020.

49. R. Hai *et al.*, "Comparative study on self-absorption of laser-induced tungsten plasma in air and in argon," *Optics Express*, vol. 27, no. 3, pp. 2509–2520, 2019.

50. A. Kramida, K. Olsen, and Y. Ralchenko, "NIST LIBS Database," National Institute of Standards and Technology. https://physics.nist.gov/PhysRefData/ASD/LIBS/libs-form.html (accessed Jan. 15, 2021).

51. A. Smolinska *et al.*, "Chapter 3 - general framing of low-, mid-, and high-level data fusion with examples in the life sciences," in *Data Fusion Methodology and Applications*, ser. Data Handling in Science and Technology, M. Cocchi, Ed. Elsevier, 2019, vol. 31, pp. 51 – 79. [Online]. Available: http://www.sciencedirect.com/science/article/pii/B978044463984400003X

52. K. Rammelkamp *et al.*, "Low-level libs and raman data fusion in the context of in situ mars exploration," *Journal of Raman Spectroscopy*, vol. 51, no. 9, pp. 1682–1701, 2020. [Online]. Available: https://onlinelibrary.wiley.com/doi/abs/10.1002/jrs.5615

53. J. A. Manrique-Martinez *et al.*, "Evaluation of multivariate analyses and data fusion between raman and laser-induced breakdown spectroscopy in binary mixtures and its potential for solar system exploration," *Journal of Raman Spectroscopy*, vol. 51, no. 9, pp. 1702–1717, 2020. [Online]. Available: https://onlinelibrary.wiley.com/doi/abs/10.1002/jrs.5819

54. E. Gibbons, R. Léveillé, and K. Berlo, "Data fusion of laser-induced breakdown and raman spectroscopies: Enhancing clay mineral identification," *Spectrochimica Acta Part B: Atomic Spectroscopy*, vol. 170, p. 105905, 2020. [Online]. Available: http://www.sciencedirect.com/science/article/pii/S058485471930429X

55. A. Rao, "Rapid analysis of plutonium surrogate material via hand-held laser-induced breakdown spectroscopy," M.S. thesis, Dept. Eng. Phys., Air Force Institute of Technology, Wright-Patterson AFB, OH, USA, 2020.

56. "7.1 Principal Components Regression (PCR)," The Pennsylvania State University. https://online.stat.psu.edu/stat508/lesson/7/7.1 (accessed Jan. 16, 2021).

57. K. Dunn, "6.6 Principal Component Regression (PCR)," Process Improvement Using Data. https://learnche.org/pid/latent-variable-modelling/principal-components-regression (accessed Jan. 16, 2021).

58. P. Allison, "When can you safely ignore multicollinearity?" Statistical Horizons. https://statisticalhorizons.com/multicollinearity (accessed Jan. 16, 2021).

59. P. Barbiero *et al.*, "Unsupervised gene identification in colorectal cancer," in *Smart Innovation, Systems and Technologies*, New York City, NY, USA: Springer, 2018.

60. G. James *et al.*, *An Introduction to Statistical Learning with Applications in R*, G. Casella, S. Fiensberg, and I. Olkin, Eds. New York, NY: Springer, 2019, vol. 11, no. 4.

61. H. Abdi, "Partial Least Squares (PLS) Regression," University of Texas at Dallas, Dallas, TX, Jan. [Online]. Available: https://personal.utdallas.edu/~herve/Abdi-PLS-pretty.pdf

62. R. Junjuri and M. K. Gundawar, "A low-cost libs detection system combined with chemometrics for rapid identification of plastic waste," *Waste Management*, vol. 117, pp. 48 – 57, 2020. [Online]. Available: http://www.sciencedirect.com/science/article/pii/S0956053X20304244

63. Y.-I. Lee *et al.*, "Interaction of an Excimer-Laser Beam with Metals. Part III: The Effect of a Controlled Atmosphere in Laser-Ablated Plasma Emission," *Appl. Spectrosc.*, vol. 46, no. 11, pp. 1597–1604, Nov 1992. [Online]. Available: http://as.osa.org/abstract.cfm?URI=as-46-11-1597

64. B. Lal *et al.*, "Parametric study of pellets for elemental analysis with laser-induced breakdown spectroscopy," *Applied Optics*, vol. 43, no. 13, pp. 2792–2797, 2004.

65. W. Tawfik, "Why carbon lines intensities in LIBS are usually lower in compare to other elements like sodium?" Cairo University. https://www.researchgate.net/post/Why_carbon_lines_intensities_in_LIBS_are_usually_lower_in_compare_to_other_elements_like_sodium (accessed Jan. 29, 2021).

66. C. Basler *et al.*, "Comparison of laser pulse duration for the spatially resolved measurement of coating thickness with laser-induced breakdown spectroscopy," *Sensors*, vol. 19, p. 4133, 09 2019.

67. P. Sdvizhenskii *et al.*, "Deep ablation and libs depth elemental profiling by combining nano- and microsecond laser pulses," *Spectrochimica Acta Part B: Atomic Spectroscopy*, vol. 177, p. 106054, 2021.

68. J. P. Smith *et al.*, "Investigation of minor elemental species within tablets using in situ depth profiling via laser-induced breakdown spectroscopy hyperspectral imaging," *Spectrochimica Acta Part B: Atomic Spectroscopy*, vol. 165, p. 105769, 2020.

69. C. Ke *et al.*, "Application of laser induced breakdown spectroscopy for fast depth profiling analysis of type 316 stainless steel parts corroded by liquid lithium," *Fusion Engineering and Design*, vol. 136, pp. 1647–1652, 2018, special Issue: Proceedings of the 13th International Symposium on Fusion Nuclear Technology (ISFNT-13).

REPORT DOCUMENTATION PAGE

Form Approved
OMB No. 0704–0188

1. REPORT DATE *(DD–MM–YYYY)*	2. REPORT TYPE	3. DATES COVERED *(From — To)*
25–03–2021	Master's Thesis	May 2019 — Mar 2021

4. TITLE AND SUBTITLE

Lithium Compound Characterization via Raman Spectroscopy and Laser-Induced Breakdown Spectroscopy

5a. CONTRACT NUMBER

5b. GRANT NUMBER

5c. PROGRAM ELEMENT NUMBER

6. AUTHOR(S)

Stofel, James T., Capt, USAF

5d. PROJECT NUMBER

XXXXXX

5e. TASK NUMBER

5f. WORK UNIT NUMBER

7. PERFORMING ORGANIZATION NAME(S) AND ADDRESS(ES)

Air Force Institute of Technology
Graduate School of Engineering an Management (AFIT/EN)
2950 Hobson Way
WPAFB OH 45433-7765

8. PERFORMING ORGANIZATION REPORT NUMBER

AFIT-ENG-MS-21-M-138

9. SPONSORING / MONITORING AGENCY NAME(S) AND ADDRESS(ES)

Air Force Technical Applications Center

10. SPONSOR/MONITOR'S ACRONYM(S)

AFTAC

11. SPONSOR/MONITOR'S REPORT NUMBER(S)

12. DISTRIBUTION / AVAILABILITY STATEMENT

DISTRIBUTION STATEMENT A:
APPROVED FOR PUBLIC RELEASE; DISTRIBUTION UNLIMITED.

13. SUPPLEMENTARY NOTES

14. ABSTRACT

Industries such as lithium-ion battery producers and the nuclear industry community seek to produce and store lithium in pure chemical forms. However, these lithium compounds are reactive with the atmosphere and quickly degrade into less desirable forms. Therefore, industry desires a fast and effective quality control approach to quantify the ingrowth of these secondary lithium chemical forms. This research presents a novel approach using Laser-Induced Breakdown Spectroscopy (LIBS) and Raman spectroscopy in tandem to enhance lithium compound characterization beyond what is achieved by either technique alone. The resulting spectral data are aggregated using data fusion and analyzed using chemometrics for the first time. Additionally, LIBS and Raman spectra are analyzed individually using chemometrics and a comparison is made between the techniques individually and the fused data. It is determined the presence of lithium compounds is best characterized using fused LIBS-Raman data analyzed with partial least squares regression.

15. SUBJECT TERMS

Lithium, Raman, LIBS

16. SECURITY CLASSIFICATION OF:			17. LIMITATION OF ABSTRACT	18. NUMBER OF PAGES	19a. NAME OF RESPONSIBLE PERSON
a. REPORT	b. ABSTRACT	c. THIS PAGE			LTC Michael Shattan, AFIT/ENP
U	U	U	UU	91	19b. TELEPHONE NUMBER *(include area code)* 937-255-3636 x4587; michael.shattan@afit.edu